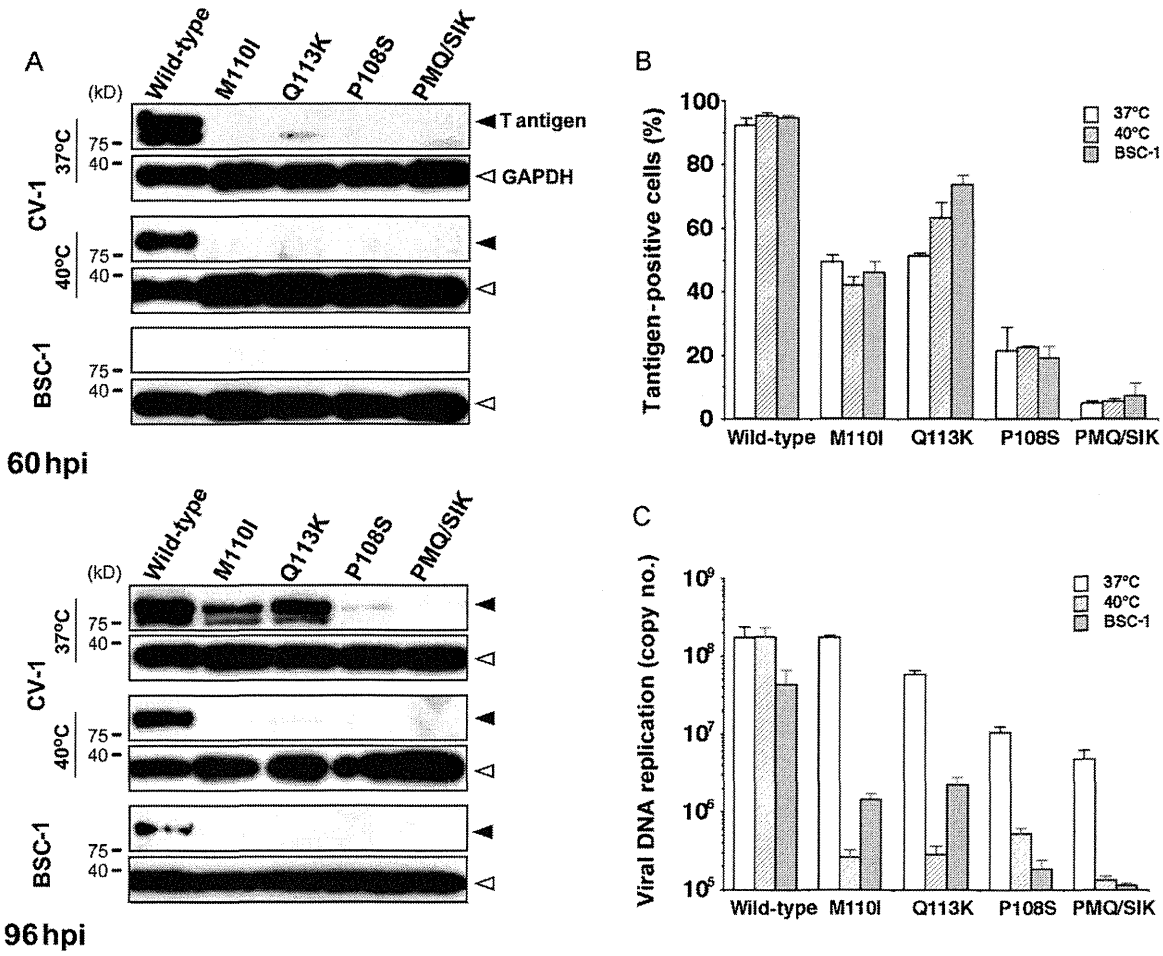

Fig. 2. Viral gene expression and viral DNA replication of mutants harboring tsD mutations. (A) Western blot detection of T antigen expression on infection with mutants: CV-1 or BSC-1 cells infected with either wild-type or the mutant were harvested for detecting the T antigen by Western blot at 60 h hpi (upper panel) or 96 hpi (lower panel). Approximately half of the cells harvested from individual six-well plates were used for detecting the SV40 T antigen using mouse monoclonal anti-T antigen (PAb419; Oncogene Sci., USA) as the primary antibody and peroxidase-conjugated anti-mouse IgG antibody (GE Healthcare, Bucks, UK) as the secondary antibody followed by enzyme chemiluminescence (ECL) (Immunostar; Wako chemicals, Osaka, Japan). As a loading control, glyceraldehyde-3-phosphate dehydrogenase (GAPDH) was detected using mouse anti-GAPDH antibody (clone 6C5; Millipore, Billerica, MA, USA) by ECL similar to the T antigen. Note that wild-type-infected cells tended to have lower amounts of protein because of an effective blockage of cell growth on infection, whereas the mutant-infected cells were less interfered with the growth likely due to lower incident of viral infection or lower level of viral gene expression. Positions of molecular weight markers for 75 and 45 kDa as well as those of the T antigen (filled arrowhead) and GAPDH (open arrowhead) are indicated. (B) Immunofluorescence detection of T antigen expression on infection: Cell lysates containing viral particles, adjusted for viral DNA as in the plaque assay (Fig. 1B), were used to infect CV-1 cells incubated at 37 °C (open columns) or 40 °C (shaded columns), and to BSC-1 cells incubated at 37 °C (closed columns). At 60 hpi, the cells were fixed, and the proportion of T antigen-positive cells were examined by immunocytochemistry using mouse monoclonal anti-T antigen antibody and Alexa Fluor 488-conjugated goat anti-mouse IgG antibody (Molecular probes, Eugene, OR, USA). (C) Viral DNA replication on infection with mutants: The cells infected as described in Fig. 2B were extracted for low molecular weight DNA at 96 hpi as described (Nakanishi et al., 2006). The extracted DNA was quantified for SV40 DNA as described in Fig. 1B. The columns are designated as shown in Fig. 2B. The amount of viral DNA shown is the mean value of the triplicate with standard deviation as indicated.

with those obtained by Western blot detection of T antigen expression (Fig. 2A, upper panel).

When T antigen expression was examined for the lysate obtained at 96 hpi by Western blot, the comparable signal was detected in wild-type-, M110I-, and Q113K-infected CV-1 cells grown at permissive temperature. The lysate from wild-type-infected CV-1 cells grown at 40 °C and BSC-1 cells at 37 °C also contained detectable T antigen, while the signal was mostly undetected in mutant-infected CV-1 cells grown at 40 °C and in BSC-1 cells. Similarly, the extent of viral DNA replication examined by quantitative PCR showed that the levels of viral DNA in M110I- and Q113K-infected CV-1 cells grown at 37 °C were comparable with those in wild-type-infected cells, while a much lower extent of DNA replication was observed when the cells were incubated at 40 °C or in BSC-1 cells infected with the respective mutants (Fig. 2C). The growth of the mutants P108S and PMQ/SIK was affected by the mutation in CV-1 cells even grown at 37 °C and severely blocked at 40 °C and in BSC-1 cells. We note that viral growth in mutant-infected BSC-1 cells was similar to that in mutant-infected CV-1 cells at non-permissive temperature. Viral DNA replication in BSC-1 cells is known to be initiated 10–20 h later than that in CV-1 cells (Ritzi and Levine, 1970). Such slower viral growth in BSC-1 cells could make the mutants' growth defect more apparent similar to that in CV-1 cells grown at 40 °C. These results indicated that, similar to the previous observations using the mutants with natural SV40 backbone, the mutants showed growth defect in CV-1 cells at non-permissive temperature and in BSC-1 cells. P108S mutation appeared to affect viral gene expression and DNA replication more severely than M110I and Q113K mutations.

The VP4 ORF status differs among the mutants. tsD101 (Q113K) harbors the VP4 Gln 4 to Lys alteration, and tsD222 (M110I) harbors no VP4 ORF because of alteration in the initiation codon, whereas the tsD202 (P108S) VP4 ORF is unaffected by the mutation (Fig. 1). Chou and Martin (1974) showed that coinfection of

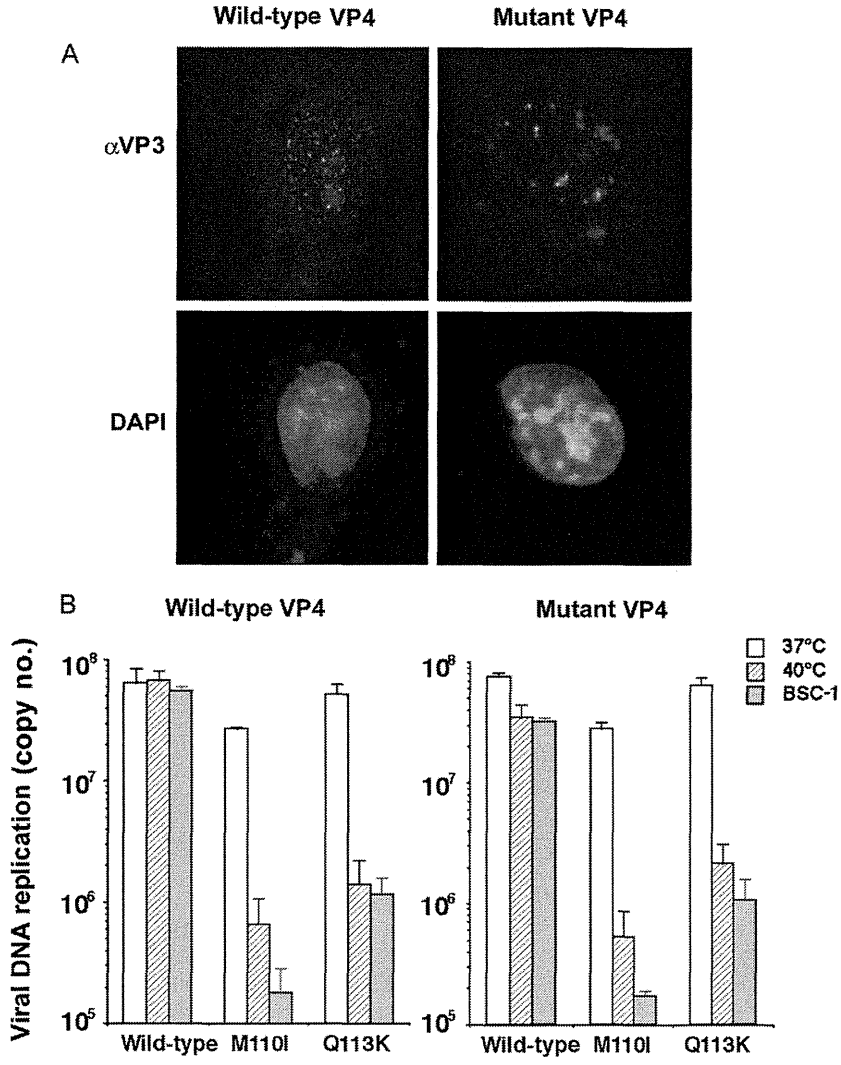

Fig. 3. VP4 complementation to mutant-infected cells. (A) Immunofluorescence detection of VP4 expressed from the VP4 expression vector: BSC-1 cells grown on coverslip were transfected with pSCMV VP4w or pSCMV VP4q using Lipofectamine 2000 (Invitrogen, Carlsbad, CA, USA) following the manufacturer's instruction. Cells were fixed at 48-h after transfection with acetone–methanol and stained for VP4 using rabbit anti-VP3 antibody (Abcam, Cambridge, UK) followed by Alexa Fluor 555-conjugated goat anti-rabbit IgG antibody (Molecular probes, Eugene, OR, USA). 4′,6-diamidino-2-phenylindole (DAPI) was used to counterstain for visualizing the cell nucleus. Identical set of cells showing representative images observed under the epifluorescent microscope are shown. (B) Viral DNA replication on VP4 complementation: CV-1 or BSC-1 cells grown in six-well plates were applied with approximately 1000 viral particles and approximately 1000 SV40 vectors carrying the VP4 expression vector to each cell. Viral DNA found in the cells coinfected with the vector carrying either pSCMV VP4w (left panel: Wild-type VP4) or pSCMV VP4q (right panel: Mutant VP4) incubated at designated temperature at 96 hpi was quantified for viral DNA as shown in Fig. 1B. The columns are marked as shown in Fig. 2B.

tsD202 and tsD222 or tsD101 at the non-permissive temperature did not complement the plaque forming-activity, showing that each pair of mutants harbor a genetically indistinguishable defect. Similarly, coinfection of CV-1 cells with Q113K and M110I with a natural SV40 backbone at 40 °C did not change their plaque-forming activity, confirming that the mutants belong to the same complementation group and their defects are genetically indistinguishable (Supplemental Table S1). When the mutations were combined, exemplified in the PMQ/SIK mutant, growth was more severely affected than those in the original mutants (Fig. 1B), suggesting that the gathered mutations had a cumulative impact on viral growth.

We examined by Western blot the presence or absence of VP4 in CV-1 and BSC-1 cells infected with their respective mutants. However, multiple attempts to detect VP4 using an antibody similar to that used in the original report (Daniels et al., 2007) (and provided by the same source) as well as a commercially available antibody (Anti-VP2/3; Abcam, Cambridge, UK) were unsuccessful. The VP3 proteins appeared to be highly prone to partial digestion in the cell, and proteins smaller than VP3 (approximately 25, 18, 16, and 12 kDa) that were reactive to the antibody were frequently detected in the virus-infected cells, causing difficulty in identifying the VP4 band (data not shown). We also examined VP4 ORF by *in vitro* translation using the PCR fragments harboring the VP3 coding region of either wild-type's or the mutants'. We did find VP4-like band, though very faint, that appeared in the *in vitro* translation of the wild-type VP3 coding region but not in those harboring M110I mutation (Supplemental Fig. S3). Instead of pursuing VP4 detection, we examined whether lack of VP4 is the cause of the growth defect at non-permissive temperatures in CV-1 cells or of the reduced infectivity in BSC-1 cells, i.e., whether supplying VP4 to mutant-infected cells would restore viral growth. To this end, we made the VP4 expression vectors pSCMV VP4w and pSCMV VP4q carrying wild-type VP4 ORF and VP4 ORF with VP3 Q113K (VP4 Q4K) mutation, respectively. Briefly, the ZsGreen coding region of pSCMV-ZG (Nakanishi

et al., 2008) was replaced with that of VP4 ORFs amplified by PCR using NOpSV40 or NOpSV40 Q113K as the template and the primers

5′-GGCCCGGGATCCACCGGTCGCCACCATGGTGAGACAAGTAGCC-3′

and 5′-TCTAGAGGGTCGTGTACATTAACTC-3′ (restriction sites are underlined) using the *AgeI* and *BsrGI* sites. The constructs harbor the human cytomegalovirus immediate-early promoter and SV40 origin that drives expression of VP4, introduced with a strong ATG context (boxed sequence in the primer) for ensuring VP4 translation, and are also available for packaging to the SV40 vector because of the presence of the SV40 origin (Nakanishi et al., 2008). On transfection of the constructs into BSC-1 cells followed by immunofluorescence detection of VP4 using anti-VP3 antibody, positive signals seen as nuclear dots, similar to those reported previously (Daniels et al., 2007), were evident (Fig. 3A). SV40 vectors packaging pSCMV VP4w or VP4q were then made by cotransfection of 293T cells with pCAG SV40, pCI Ts, and either pSCMV VP4w or VP4q, purified for the SV40 vector by 27–39% Optiprep gradient sedimentation (Nakanishi et al., 2008). The vectors were transduced into CV-1 or BSC-1 cells and coinfected with the viral particles either of wild-type, M110I, or Q113K. The cells were then examined for the extent of viral DNA replication at 96 hpi using quantitative real-time PCR (Fig. 3B). On coinfection with the VP4 vector expressing wild-type or mutant VP4, the extent of viral DNA replication did not recover in mutant-infected CV-1 cells incubated at non-permissive temperature as well as in mutant-infected BSC-1 cells; the profile of viral growth defect was unchanged with or without wild-type VP4 transduction by the VP4 expression vector. The results suggested that presence of wild-type or mutant VP4 did not complement the growth defect of the mutants and was consistent with the idea that these growth defects occur in the early stages of infection.

Here we report that the tsD222 mutant is identical to VP2 M228I, known to be defective in expressing VP4 (Daniels et al., 2007), though the mutant showed a conditional temperature growth phenotype in CV-1 cells. Genetic complementation studies confirmed that the growth defect was not related to the absence of an intact VP4 ORF, since the growth of tsD101 (Q113K), in which VP4's fourth amino acid was altered from Gln to Lys, and tsD202 (P108S), in which VP4 ORF was intact, was also affected, and they did not genetically complement each other. The mutants in the context of a natural genome as well as in the context of an NOSV40 viral genome, in which the overlapping coding regions of VP2/3 and VP1 are separated by a duplication of the overlapping region, exhibited similar phenotypes with a temperature-sensitive growth defect in CV-1 cells and the inability to genetically complement each other (Supplemental Table S1 and data not shown). Consistent with these results, supplying VP4 *in trans* using the VP4 expression vector did not ameliorate the mutants' growth at non-permissive temperatures and in BSC-1 cells (Fig. 3). Since viral gene expression and DNA replication were affected by the mutations, our results indicated that the defect in the mutants involves one or more defects in VP2/3. This is reasonable given that VP4 is a nonstructural protein that is expressed in the very late stage of infection and thus mediating viral spread, which is the major role of VP4 (Daniels et al., 2007). Thus, the effect of tsD mutation is more significant in the early stages of viral infection during viral propagation, and a defect in mutant VP2/3 made a more significant contribution to the temperature-sensitive phenotype than the absence of a functional VP4.

Acknowledgments

We thank Dr. Ariella Oppenheim (Hebrew University) for the generous gift of anti-VP3 anti-serum, and Dr. Harumi Kasamatsu (University of California, Los Angeles) and Dr. Mary J. Tevethia (Pennsylvania State University) for providing the viral lysates of tsD101, tsD202, and tsD222. This work was supported by a Grant-in-Aid for Scientific Research from Japan Society for the Promotion of Science and Health Labor Sciences Research Grant on "Research on Emerging and Re-emerging Infectious Diseases" to AN.

Appendix A. Supplementary data

Supplementary data associated with this article can be found, in the online version, at doi:10.1016/j.virusres.2011.02.001.

References

Avila, J., Saral, R., Martin, R.G., Khoury, G., 1976. The temperature-sensitive defect in SV40 group D mutants. Virology 73 (1), 89–95.
Chen, X.S., Stehle, T., Harrison, S.C., 1998. Interaction of polyomavirus internal protein VP2 with the major capsid protein VP1 and implications for participation of VP2 in viral entry. EMBO J. 17 (12), 3233–3240.
Chou, J.Y., Avila, J., Martin, R.G., 1974. Viral DNA synthesis in cells infected by temperature-sensitive mutants of simian virus 40. J. Virol. 14 (1), 116–124.
Chou, J.Y., Martin, R.G., 1974. Complementation analysis of simian virus 40 mutants. J. Virol. 13 (5), 1101–1109.
Chou, J.Y., Martin, R.G., 1975. DNA infectivity and the induction of host DNA synthesis with temperature-sensitive mutants of simian virus 40. J. Virol. 15 (1), 145–150.
Daniels, R., Sadowicz, D., Hebert, D.N., 2007. A very late viral protein triggers the lytic release of SV40. PLoS Pathog. 3 (7), e98.
Ishii, N., Nakanishi, A., Yamada, M., Macalalad, M.H., Kasamatsu, H., 1994. Functional complementation of nuclear targeting-defective mutants of simian virus 40 structural proteins. J. Virol. 68 (12), 8209–8216.
Lai, C.J., Nathans, D., 1975a. A map of temperature-sensitive mutants of simian virus 40. Virology 66 (1), 70–81.
Lai, C.J., Nathans, D., 1975b. Mapping the genes of simian virus 40. Cold. Spring. Harb. Sympos. Quant. Biol. 39 (Pt. 1), 53–60.
Li, P.P., Naknanishi, A., Tran, M.A., Ishizu, K., Kawano, M., Phillips, M., Handa, H., Liddington, R.C., Kasamatsu, H., 2003. Importance of Vp1 calcium-binding residues in assembly, cell entry, and nuclear entry of simian virus 40. J. Virol. 77 (13), 7527–7538.
Nakanishi, A., Chapellier, B., Maekawa, N., Hiramoto, M., Kuge, T., Takahashi, R.U., Handa, H., Imai, T., 2008. SV40 vectors carrying minimal sequence of viral origin with exchangeable capsids. Virology 379 (1), 110–117.
Nakanishi, A., Nakamura, A., Liddington, R., Kasamatsu, H., 2006. Identification of amino acid residues within simian virus 40 capsid proteins Vp1, Vp2, and Vp3 that are required for their interaction and for viral infection. J. Virol. 80 (18), 8891–8898.
Nakanishi, A., Shum, D., Morioka, H., Otsuka, E., Kasamatsu, H., 2002. Interaction of the Vp3 nuclear localization signal with the importin alpha 2/beta heterodimer directs nuclear entry of infecting simian virus 40. J. Virol. 76 (18), 9368–9377.
Reddy, V.B., Thimmappaya, B., Dhar, R., Subramanian, K.N., Zain, B.S., Pan, J., Ghosh, P.K., Celma, M.L., Weissman, S.M., 1978. The genome of simian virus 40. Science 200 (4341), 494–502.
Ritzi, E., Levine, A.J., 1970. Deoxyribonucleic acid replication in simian virus 40-infected cells. III. Comparison of simian virus 40 lytic infection in three different monkey kidney cell lines. J. Virol. 5 (6), 686–692.
Robb, J.A., Martin, R.G., 1972. Genetic analysis of simian virus 40.3. Characterization of a temperature-sensitive mutant blocked at an early stage of productive infection in monkey cells. J. Virol. 9 (6), 956–968.
Shenk, T.E., Rhodes, C., Rigby, P.W., Berg, P., 1975. Mapping of mutational alterations in DNA with S1 nuclease: the location of deletions, insertions and temperature-sensitive mutations in SV40. Cold. Spring. Harb. Symp. Quant. Biol. 39 (Pt. 1), 61–67.

Virology 412 (2011) 179–187

Contents lists available at ScienceDirect

Virology

journal homepage: www.elsevier.com/locate/yviro

Novel DNA virus isolated from samples showing endothelial cell necrosis in the Japanese eel, *Anguilla japonica*

Tetsuya Mizutani [a,*,1], Yusuke Sayama [a,b,1], Akira Nakanishi [c,1], Hideharu Ochiai [d], Kouji Sakai [e], Kouji Wakabayashi [f,2], Nozomi Tanaka [f], Emi Miura [f], Mami Oba [a], Ichiro Kurane [a], Masayuki Saijo [a], Shigeru Morikawa [a], Shin-ichi Ono [f,*]

[a] *Virology 1, National Institute of Infectious Diseases, Gakuen 4-7-1, Musashimurayama, Tokyo 208-0011, Japan*
[b] *Department of Virology, Tohoku University School of Medicine, 2-1 Seiryo-machi, Aoba-ku, Sendai 980-8575, Japan*
[c] *National Center for Geriatrics and Gerontology, 35 Gengo, Morioka-machi, Obu, Aichi 474-8522, Japan*
[d] *Research Institute of Biosciences, Azabu University, Fuchinobe 1-17-71, Chuo-ku, Sagamihara, Kanagawa 252-5201, Japan*
[e] *Division of Experimental Animals Research, National Institute of Infectious Diseases, 4-7-1 Gakuen, Musashi-Murayama, Tokyo 208-0011, Japan*
[f] *School of Marine Science and Technology, Tokai University, 3-20-1 Orido, Shimizu-ku, Shizuoka 424-8610, Japan*

ARTICLE INFO

Article history:
Received 19 October 2010
Returned to author for revision
6 December 2010
Accepted 28 December 2010
Available online 1 February 2011

Keywords:
Novel DNA virus
Japanese eel endothelial cells-infecting virus
Anguilla japonica

ABSTRACT

Economic loss due to viral endothelial cell necrosis of eel (VECNE) of *Anguilla japonica* is a serious problem for the cultured Japanese eel market. However, the viral genome responsible for VECNE is unknown. We recently developed a rapid determination system for viral nucleic acid sequences (RDV) to determine viral genome sequences. In this study, viral DNA fragments were obtained using RDV, and approximately 15-kbp circular full genome sequences were determined using a next-generation sequencing system, overlapping PCR, and Southern blot analysis. One open reading frame (ORF) was homologous to the large T-antigen of polyomavirus; other ORFs have no homology with any nucleic or amino acid sequences of polyomavirus. Therefore, as this DNA virus might comprise a novel virus family, we provisionally named it Japanese eel endothelial cells-infecting virus (JEECV). JEECV was detected in both naturally and experimentally infected eels, suggesting that JEECV potentially causes VECNE.

Introduction

The Japanese eel *Anguilla japonica* is an important fish species in several Asian countries including Japan. Viral endothelial cell necrosis of eel (VECNE) of *A. japonica* is a serious problem in Japanese aquaculture industry (Egusa et al, 1989; Inoue et al, 1994; Ono and Nagai, 1997). In Shizuoka, a prefecture where the eel is mass-produced, the total production of Japanese eel was approximately 1700 tons (4 billion yen), and 107 tons worth of eel died from illness in 2008. Of these 107, 31 tons worth of the eels died from VECNE. Thus, economic loss due to VECNE is a serious problem in the cultured eel business. To prevent the spread of VECNE, obtaining genomic information of the unknown viral agent is crucial for developing a detection system and vaccines.

We and other groups reported that VECNE occurs naturally (Egusa et al, 1989; Inoue et al, 1994; Ono and Nagai, 1997). Naturally VECNE shows reddening of fins with a swollen abdomen. Intense congestion occurs in the gills, liver, and intestine. Histopathology of VECNE is characterized by intense congestion in the central venous sinuses of the gill filaments compared to healthy eels. This pathological change is accompanied by degeneration of nuclei of endothelial cell in blood vessels; this degeneration is characterized by swelling. Hexagonal virus particles measuring about 75 nm in diameter were observed in the nuclei. Thus, VECNE results from a systemic viral infection that causes necrosis of endothelial cells in blood vessels. VECNE was experimentally induced by injecting a filtered homogenized solution of diseased eels into the abdominal cavities of healthy eels (Ono and Nagai, 1997). Since the first report regarding VECNE was published in 1989 (Egusa et al, 1989), the causative virus has not been identified because cell culture systems for viral isolation are not available. Therefore, we established a cell line that originated from vascular endothelial cells of *A. japonica* (Ono et al, 2007). The primary Japanese eel endothelial (JEE) cell culture system was established using the dorsal aorta and aortic bulbs of healthy eels. To isolate the causative virus, gill lamellae were homogenized and centrifuged. The supernatant was then filtered using a 0.45-μm filter. The filtrate was added to JEE cells. At 7 days post-inoculation (p.i.), cytopathic effect (CPE) with markedly hypertrophied nuclei was observed (Ono et al, 2007). After a second passage, CPE was observed at 4 days p.i. Serial passages of the virus in JEE cells also induced CPE. When JEE cells were treated with 5-iodo-2′-deoxyuridine before virus inoculation, CPE was inhibited, strongly suggesting that the virus has DNA as its genome. In addition, this virus exhibited chloroform

* Corresponding authors. T. Mizutani is to be contacted at Fax: +81 425 65 3315.
E-mail address: tmizutan@nih.go.jp (T. Mizutani).
[1] These authors contributed equally to this study.
[2] Present address: International Pet World College, Niigata, 950-0911, Japan.

0042-6822/$ – see front matter © 2011 Elsevier Inc. All rights reserved.
doi:10.1016/j.virol.2010.12.057

resistance, suggesting it is not an envelope virus. The shape of this virus in JEE cells is the same as that in naturally infected eels, as confirmed by electron microscopy (EM). The isolated virus caused VECNE in eels, as determined by a previous study (Ono et al, 2007). Although this virus was believed to be an adenovirus-like virus from these data, nucleic acid sequences were not determined.

We recently developed a rapid determination system for viral nucleic acid sequences (called RDV) to determine viral genomic sequences without cloning in a plasmid vector (Mizutani et al, 2007). RDV allows for exhaustive identification of viruses compared to previous virus detection systems, such as RT-PCR, because it does not require specific primers for target virus nucleotide sequences. In previous studies, we identified several novel viruses, such as Ryukyu virus 1 (bat adenovirus) (Maeda et al, 2008), *Hipposideros diadema* herpesvirus 1 (from bat) (Watanabe et al, 2009), Bat betaherpesvirus 2 (Watanabe et al., in press), Ostrich virus 1 (orthoreovirus) (Sakai et al, 2009) and Phasi Charoen virus (mosquito bunyavirus) (Yamao et al, 2009). In this study, we used RDV with the supernatant of virus-infected JEE cells to obtain viral genomic sequences of the viruses infecting JEE cells.

Results

Virus shape in virus stock analyzed using EM

To confirm that the virus stocks (supernatant of virus-infected cells) cause VECNE in eels, 70th-passage virus stock was used in this study. Virus shapes were observed in the nuclei using electron microscopy (EM) (Fig. 1A and B) after JEE cells were infected with the virus stock. After filtering the virus stock using 0.45-μm filters, the virus was inoculated into eels. EM photographs of the gill are illustrated in Fig. 1C and D. Intense congestion occurred in the gill (Fig. 1E) and liver (Fig. 1F) at 8 days p.i. Although we evaluated a number of EM photographs of JEE cells and gills, we found only one species based on virus shape. This suggests that the virus stock over 70 passages in JEE cells contain agent(s) causing VECNE.

Partial viral genomic DNA sequences using RDV

To obtain viral DNA genomic sequences, DNA was extracted from the supernatant of virus-infected JEE cells at 4 days p.i. after RNase A and DNase I treatment. RDV was then performed. A total of 29 PCR products were extracted from agarose gels at the final step of RDV, and direct sequencing was performed. The nucleotide sequences were used to determine homologous sequences using BLASTx and tBLAST at the National Center for Biotechnology Information (NCBI) web site. Nine read sequences were not homologous to any genes. PCR primers were designed based on these sequences, and three read sequences (read-024, -004A, and -004C) were amplified in virus-infected cells, but not in mock-infected cells, using DNA samples (Fig. 2A). One read sequence, read-024, comprising 100 amino acids were homologous to the sequence of the large T-antigen of polyomaviruses, such as budgerigar fledgling disease virus and human polyomaviruses. Read-024 was detected using RT-PCR using the RNA extracted from virus-infected cells at 3 days p.i. (Fig. 2B), indicating that it was transcribed in infected cells. In addition, 16S ribosomal DNA of bacteria and mycoplasma was not detected in these DNA samples using PCR (data not shown). These results indicated that these read sequences obtained using RDV were parts of the viral genome.

Elongation of viral genomic sequences

Based on these viral nucleotide sequences, genome walking was performed using differential display RT-PCR (GeneFishing DEG Premix Kit; Seegene). We obtained DNA fragments of 5 and 2 kbp approximately. To obtain the entire genome sequence of this virus, we used the Genome Sequencer FLX System (Titanium) of Roche and 454 Life Sciences. Viral DNA was extracted by precipitation of 30-ml virus-infected cell supernatant at 4 days p.i using ultracentrifugation. The obtained 17,000 read sequences were analyzed using the GS *De novo* Assembler Version 2.3 (Roche) for *de novo* assembly. As a result, we obtained 15,131 total nucleotides with circular DNA forms comprising this viral genome (Fig. 3A). The viral genomic information was deposited in DDBJ/EMBL/GenBank (accession number AB543063). Organization of the viral genome is illustrated in Fig. 3B. Because we could not find a motif of replicative origin on this genome, the provisional nucleotide number is 1 in Fig. 3A and B. The locations of partial DNA fragments (read-024, -004A, and -004C) obtained using RDV and two long DNA fragments (5 and 2 kbp) obtained using genome walking are also illustrated in Fig. 3B. In addition, at least 15 predicted ORFs were found in both strands using GeneMark.hmm 2.0 (Fig. 3B). These ORFs, except for the large T-antigen-like ORFs, are not homologous to any genes of polyomavirus.

Regions homologous to polyomaviruses

The DNA sequence harbored an ORF encoding 698 amino acids; a region of this reading frame contains approximately 100 amino acids as determined using RDV. This ORF is homologous to the large T-antigen gene of avian polyomaviruses at ATP-binding region (E value of 8e-54) (Fig. 4A and B), although it is distinct from the usual configuration of polyomaviral T-antigen genes. Usually, T-antigen genes carry an intron in the middle of the sequence having one splice donor and two splicing acceptors, allowing alternative splicing to produce mRNA for large and small T-antigens. In contrast, the ORF appeared contiguous without introns, suggesting that the DNA is not a direct descendent of a polyomaviral DNA and likely belongs to a novel virus family. We provisionally named this DNA as JEE cells-infecting virus (JEECV).

Multiplicity of JEECV in JEE cells

To investigate multiplicity of JEECV in JEE cells, a TaqMan real-time PCR system was developed. Probe and primers were designed for the large T-antigen-like region. The virus stock at 0.01 $TCID_{50}$/cell multiplicity of infection (MOI) was inoculated into confluent JEE cells in a 24-well plate, and cells and supernatant were harvested at 24, 48, 72, 96, 120, 144, 163, and 187 h p.i. As illustrated in Fig. 5A, viral gene numbers increased in the cells and supernatant from 24 to 144 h p.i. Conventional PCR was also performed, and similar results were obtained (Fig. 5B).

Demonstration of intact genome size of JEECV

As illustrated in Fig. 3, 454 analysis revealed that JEECV genome is circular. We then performed rolling circle analysis for amplifying circular viral genomes (Johne, 2009). DNA extracted from the supernatant of virus-infected cells at 163 h p.i. (Fig. 4) was amplified using Phi29 enzymes (Templiphi) for circular DNA, and viral copy numbers were calculated for amplified products using real-time PCR (Fig. 4A). As a result, products of Templiphi were amplified approximately 128-fold compared with unamplified DNA (data not shown).

The reads using the next-generation sequencer were obtained as contiguous sequences (data not shown). To confirm that the circular viral genome exists, overlapping PCR on the viral genome was performed. DNA extracted from JEECV-infected cells was amplified using long PCR by overlapping the amplified region. As illustrated in Fig. 6A, we obtained PCR products at expected sizes. We confirmed the nucleotide sequences of bands after gel purification. This result suggests the presence of a circular viral genome in infected cells. In the viral genomic sequence, a repeat region is observed at 480–853 nt. The repeat region was sequenced within the long PCR product. Although we deposited a viral genomic sequence with three repeats in

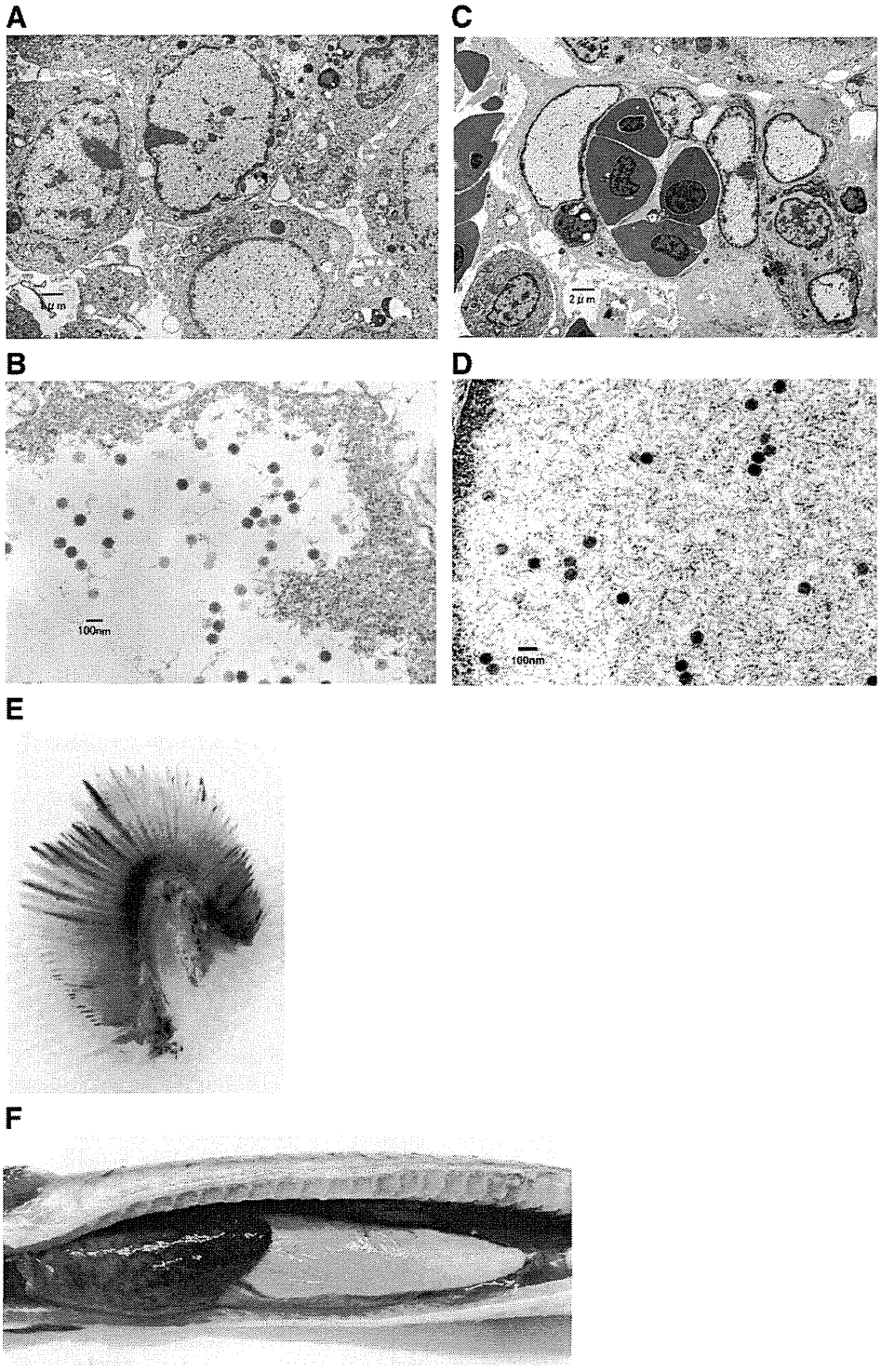

Fig. 1. Virus passage in JEE cells and infection in eels. 70th passage virus stock was infected to JEE cells (A and B) and healthy eel (C and D). EM photographs of B and D illustrate the enlarged images of A and C, respectively. Panels E and F illustrate gills and livers of virus-infected eel, respectively.

GenBank, we also detected two repeats using PCR (data not shown). Therefore, there should be different repeat numbers in virus-infected cells.

To further confirm the genomic DNA size of JEECV, we performed Southern blot analysis. DNA was digested using the restriction enzyme *BglII*, which is expected to induce a single cut in the viral genome at a position of 14418 nt. As indicated in Fig. 6B, a single band was found at approximately 15 kbp for *BglII*-digested DNA. Further confirmation is required with regard to the appropriate size for such large molecules of DNA. Another large-size DNA from nondigested DNA was observed after long exposure of the X-ray film. This band may represent another form of JEECV.

Detection of JEECV in eels

To confirm the infection of eels with JEECV, DNA was extracted from the gills of eels with natural VECNE and used to experimentally infect eels. PCR was performed for amplifying three different regions

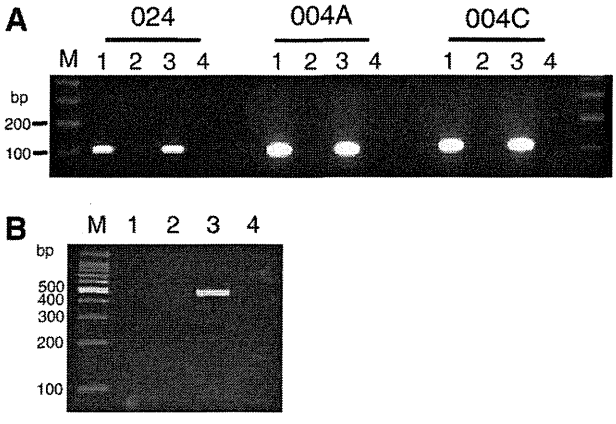

Fig. 2. Determination of viral genome sequence. A. Detection of viral DNA fragments. Three unknown DNA fragments (004A, 004C, and 024) are obtained using RDV. Primers are designed (004A-1 and -2, 004C-1 and -2, 024-3 and -4), and PCR is performed using the supernatant of virus-infected cultured cells at 7 days p.i. M, 100-bp DNA ladder marker; lane 1, supernatant of JEECV-infected cells; lane 2, supernatant of mock-infected cells; lane 3, JEECV-infected cells; lane 4, mock-infected cells. B. Detection of viral transcript. RT-PCR is performed using RNA extracted from virus-infected cells at 3 days p.i. to detect viral transcripts of the region harboring read-024 using PCR primers, 024-2 and 024-5. M, 100-bp DNA ladder marker; lanes 1 and 2, mock-infected cells; and lanes 3 and 4, JEECV-infected cells. Reaction of cDNA synthesis in lanes 2 and 4 is performed without Superscript III enzyme.

of viral genome. As illustrated in Fig. 7, viral genes were amplified in eels with natural VECNE and virus-infected eels, but not in healthy eels. Nucleotide sequences of these PCR products were confirmed after gel purification.

Discussion

In this study, we determined the genomic sequence of a novel eel virus, JEECV, which was isolated from eels with VECNE. The virus stock used in this study contained agent(s) that cause VECNE. Our results from 454 analysis, rolling circle amplification, and overlapping PCR suggested that JEECV genome is circular. We could not determine whether linear form exists in this study. Therefore, we believe that JEECV genome has two forms, linear and circular, in virus-infected cells. In addition, it is also possible that the entire linear form of the viral genome is longer than the present length obtained using Southern blot analysis. Viral genomic sequences in this study may represent one form of JEECV.

Interestingly, JEECV DNA contains regions homologous to the large T-antigen gene of polyomaviruses at ATP binding region, suggesting that this homologous region has biological function. We also investigated that bird polyomaviral T-antigen genes were more homologous to JEECV than mammals. Among four currently known bird polyomaviruses, avian polyomavirus, goose hemorrhagic polyomavirus (GHPV), finch polyomavirus, and crow polyomavirus (John and Muller, 2007), the diseases caused by GHPV (hemorrhagic nephritis and enteritis) resemble VECNE. JEECV large T antigen-like region also contains motifs conserved among polyomavirus T-antigens: DNAJ (HPDK) motif, the canonical nuclear localization signal, and zinc finger motif. Conserved region 1 (CR1) motif was found in the C-terminus, instead of N-terminus where commonly found in the polyomaviral T-antigen (Pipas, 1992). It remains to be examined whether the T-antigen-like gene influences VECNE disease symptoms, as the T-antigen genes of polyomaviruses are known to be tumorigenic. We found that the transcript harboring the large T-antigen-like gene region was detectable, thus it is possible that the T-antigen gene product is expressed. Further investigation is needed to identify the structural and nonstructural viral protein ORFs in JEECV DNA and to determine the role of viral proteins, including the T-antigen-like gene, in the development of VECNE *in vivo*.

Recently, two novel viruses, bandicoot papillomatosis carcinomatosis virus (BPCV) 1 and 2, were detected from bandicoot (Bennett et al., 2008; Woolford et al., 2007, 2008 and 2009). These virus genomes have both T-antigens of an ancestral polyomavirus and the L1 and L2 capsid proteins of an ancestral papillomavirus. Inter-familial recombination was occurred between an ancient papillomavirus and an ancient polyomavirus more than 10 million years ago (Bennett et al., 2010). JEECV genome may also arise by recombination between a polyomavirus and a virus from unknown virus family.

We are also keen to investigate in the possibility of latent infection by JEECV in Japanese eels. Natural VECNE is occasionally observed in kidneys or liver without symptoms in gills (data not shown). It is difficult to locate diseased eels exhibiting such weak symptoms. Therefore, we believe that there are eels latently infected by JEECV exhibiting very weak symptoms.

In a previous study, mortality after viral infection was reduced by incubating infected eels for more than 3 days at 35 °C under nonfeeding conditions (Tanaka et al, 2008). However, it is not cost-effective to treat a great number of eels with this condition simultaneously. To prevent the prevalence of VECNE, a monitoring system for JEECV infection developed in this study may be useful, if JEECV indeed causes VECNE.

Materials and methods

Cells, virus and viral infection

JEE cells were cultured in a medium containing Humedia-EB2 (Kurabo, Japan) and EGM-2 (Lonza, Switzerland) on a gelatin-coated 6-cm dish at 25 °C in a 5% CO_2 incubator. JEE cells were infected with the virus stock at 0.01 $TCID_{50}$/cell MOI. At 4 or 5 days p.i., the infectious fluid was harvested. To infect the eels with the virus experimentally, 1×10^6 $TCID_{50}$ (supernatant of virus-infected cultured cells) was inoculated intraperitoneally into healthy eels. At 10 days p.i., eels were analyzed. Tissues were homogenized using BioMasher (Wako Bio. Japan), and DNA was extracted using a QIAamp DNA mini kit. The experiments using eels were performed according to the regulations of Tokai University.

Analysis using RDV (Maeda et al., 2008; Mizutani et al., 2007)

The viral infected culture supernatant (100 μl) was centrifuged at 2000*g*, 15 min, 4 °C to remove cell debris and was treated with 0.0001 μg RNase A (Qiagen), and 10-μl Turbo DNA-free DNase I (Applied Biosystems, USA) were mixed with 1× Turbo DNA-free buffer and shaken at 37 °C for 30 min. For DNA extraction, a QIAamp DNA mini kit was used according to the manufacturer's instructions. A whole-genome amplification system (WGA; Sigma-Aldrich, USA) was used according to the manufacturer's instructions. In the RDV method, AmpliTaq Gold LD (Applied Biosystems) was used to obtain a high yield of the PCR products. We mixed 4 μl 10× amplification buffer in a GenomePlex Whole Genome amplification kit (WGA1) (containing primers, but no information on sequences) containing 5-μl DNA solution, 0.25 μl AmpliTaq Gold LD, and 30.75 μl distilled water. The reaction mixture was heated at 95 °C for 9 min (for activation of AmpliTaq Gold), followed by 70 cycles of amplification consisting of an annealing step at 68 °C for 1 min, a primer extension step at 72 °C for 5 min, and a denaturation step at 94 °C for 1 min. After the first DNA library was purified using the MonoFas DNA isolation system (GL Science, Japan), DNA was digested with 40-U *Hae*III (Takara Bio Inc.) at 37 °C for 30 min, and then the digested DNA was purified using MonoFas. To construct the second cDNA library, 2.50 μl DNA solution, 0.5 μl blunt *EcoR*I–*Not*I–*Bam*HI adapter (Takara Bio Inc.), and 3 μl ligation mix (Takara Bio Inc.) were reacted at room temperature for 30 min, and then the digested DNA was isolated using MonoFas. The second cDNA library was amplified using PCR using specially designed primer sets in which six nucleotides comprised CC (*Hae*III-digested

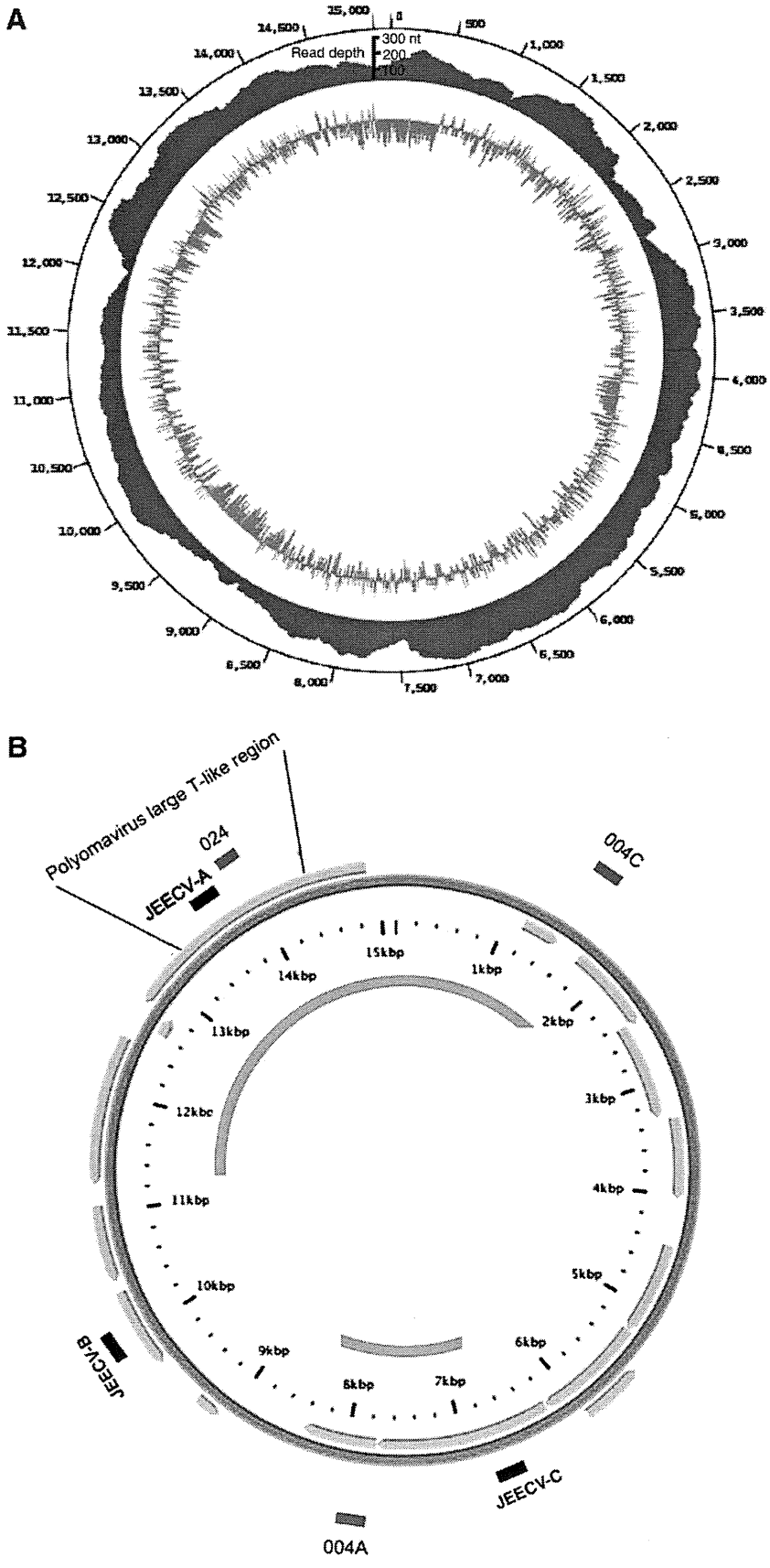

Fig. 3. Organization of the viral genome. (A) The cover depth of nucleotides analyzed using the next-generation sequencer is indicated in blue outside the JEECV genome. GC content is indicated inside the JEECV genome. Red bar, more than 50% GC content in every 10 nucleotides; green bar, less than 50% GC content. (B) Fifteen predicted ORFs are indicated with arrows. Read DNA fragments obtained using RDV and genome walking DNA fragments are indicated as blue and green lines, respectively. Black lines indicate amplified regions by PCR in Fig. 7.

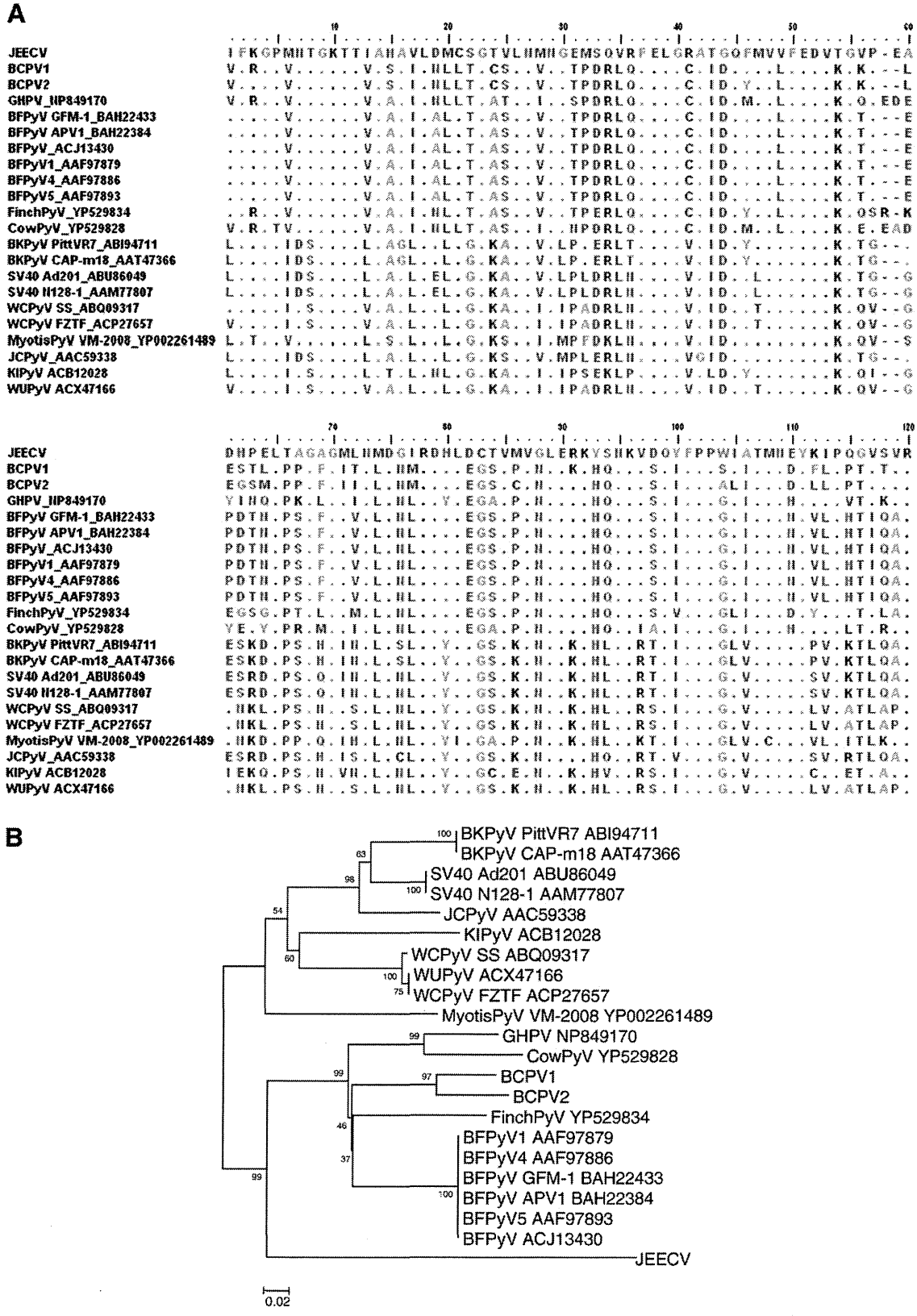

Fig. 4. Alignment of the large T-antigen-like protein. (A) Polyomavirus large T-antigen-like region of JEECV is compared with that of polyomaviruses deposited in GenBank. Alignment is performed using MEGA4 software. (B) Phylogenetic tree analysis of JEECV. The phylogenetic tree is obtained using the neighbor-joining method with 1000 bootstrap replicates, and branch length is indicated at each branch node. The horizontal scale indicates 0.02 amino acid substitutions per site. BCPV1 and 2, bandicoot papillomatosis carcinomatosis virus 1 and 2; GHPV, goose polyomavirus; BFPyV, budgerigar fledgling disease polyomavirus; finch PyV, finch polyomavirus; cow PyV, crow polyomavirus; BKPyV, BK polyomavirus; SV40, simian virus 40; WCPyV, WU polyomavirus; mytosis PyV, mytosis polyomavirus; and JCPyV, JC polyomavirus.

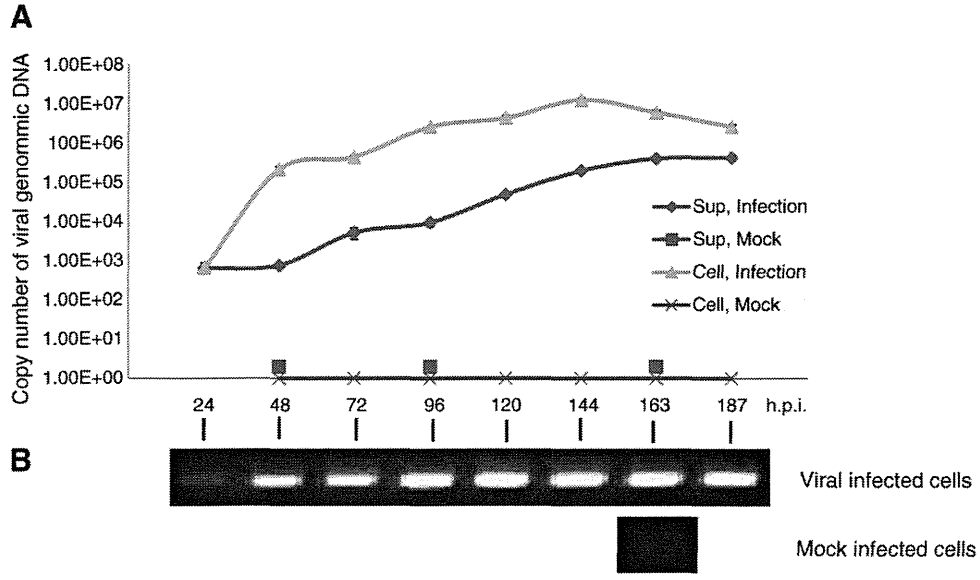

Fig. 5. Analysis of virus multiplication in JEE cells. JEECV (0.01 MOI) is infected into JEE cells. DNA extracted from cells and culture supernatant from 24 to 187 h p.i. is analyzed using real-time TaqMan PCR (A) and conventional PCR using primers, 024-3 and -4 (B).

sequence), and four variable nucleotides were added to the 3′ end of the adapter sequence. PCR was performed by mixing 15 μl AmpliTaq Gold PCR Master Mix containing AmpliTaq Gold, 0.5 μl forward primer, 0.5 μl reverse primer, 0.5 μl DNA solution, and 13.5 μl distilled water. The reaction mixture was heated at 95 °C for 12 min, followed by 70 cycles of amplification consisting of annealing and primer extension at 72 °C for 30 s and denaturation at 94 °C for 30 s. After electrophoresis of PCR products, DNA was isolated from the gel using MonoFas. Direct sequencing was performed using the forward primer and/or reverse primer.

Conventional PCR

For PCR, DNA and RNA were extracted from the supernatant and cells using the QIAamp DNA mini kit (Qiagen, USA). In this study, we used GoTaq Master Mix (Promega, USA) for conventional PCR. The

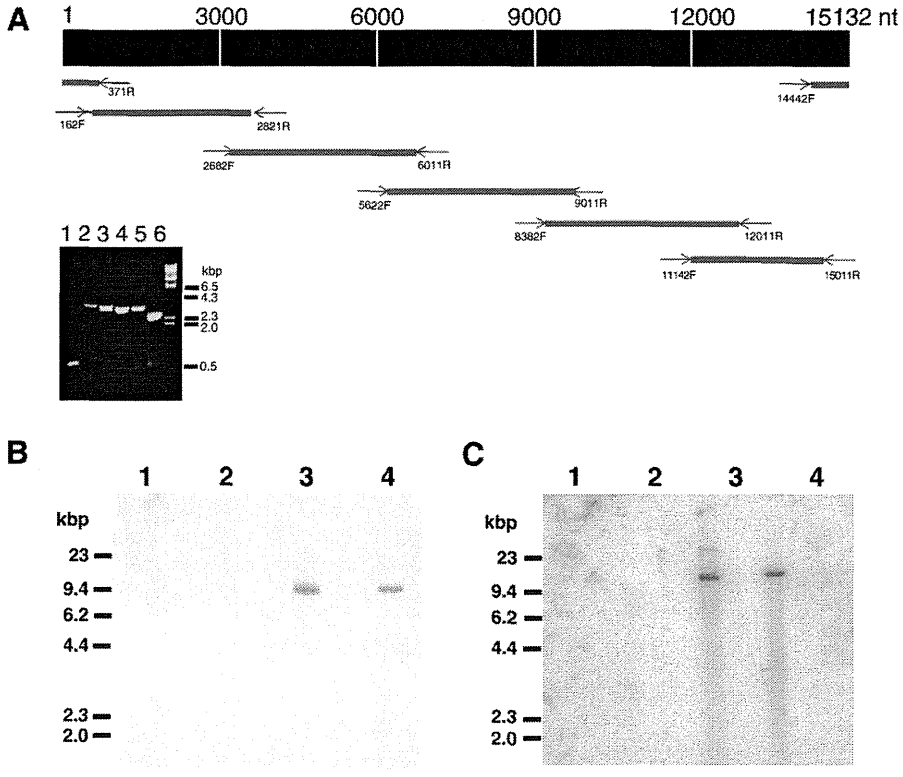

Fig. 6. Circular form of JEECV. (A) Overlapping PCR. Lane 1, 14442F and 371R primers; lane 2, 11142F and 15011R primers; lane 3, 8382F and 12011R; lane 4, 5622F and 9011R primers; lane 5, 2682F and 6011R primers; lane 6, 162F and 2821R primers. (B) Southern blot analysis with short exposure of X-ray film. (C) Southern blot analysis with long exposure using Image analyzer. Lane 1, no digested DNA from mock-infected cells; lane 2, *BglII*-digested DNA from mock-infected cells; and lane 3, no digested DNA from JJECV-infected cells; lane 4, *BglII*-digested DNA from JEECV-infected cells.

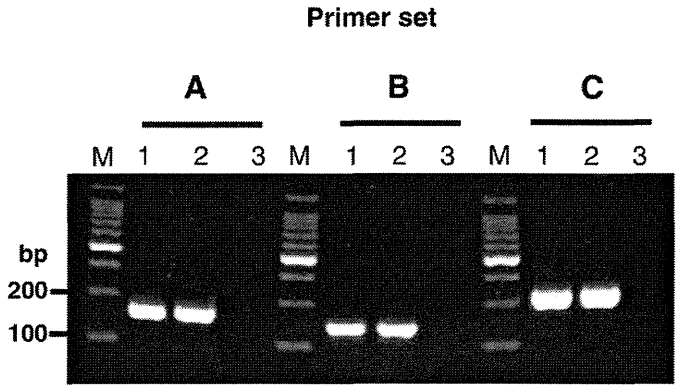

Fig. 7. Detection of JEECV in eels. Healthy eels are inoculated intraperitoneally with 1×10^6 $TCID_{50}$/cell MOI of JEECV. At 10 days p.i., DNA is extracted from gills. DNA is also extracted from gills of eel with natural VECNE and healthy eel. Conventional PCR is performed using three different primers (primer set A: JEECV-A1 and -A2, set B: JEECV-B1 and -B2, set C: JEECV-C1 and -C2). M, 100-bp DNA ladder marker; lane 1, eels with natural VECNE; lane 2, JEECV-infected eels; and lane 3, healthy eel.

reaction mixture contained 1× GoTaq Master Mix, 1 μl each of 50 μM forward and reverse primers, and template DNA. Primers are as follows:

004A-1 (5′-GGTCTCATGAAATGTAGATGTGCAGGTTAA-3′) and
004A-2 (5′-AATGCATATGAACGAGATATATACGAGC-3′) for 100-bp PCR products;
004C-1 (5′-CTCTCCGCCCTCCTGCTCATCCGGCTC-3′) and
004C-2 (5′-AATCAGACGCGCCTGAGCAGACCCAGCT-3′) for 110-bp PCR products;
024-1 (5′-TGTGATTTAGCGCAACGGCCGCAGCATA-3′) and
024-2 (5′-AGGCATCGCACATTAAACTGCACGCGCA-3′) for 240-bp PCR products; and
024-3 (5′-TACTGGTGTCTATTTGTTGCCGCACCTGC-3′) and
024-4 (5′-CAACGAACCCCGTAATTGGAATAAAGCGT-3′) for 121-bp PCR products. Usually, each PCR cycle involved denaturing at 94 °C for 2 min, annealing at 55 °C for 30 s, and primer extension at 72 °C for 30 s. This reaction was performed for 30–40 cycles. The nucleic acid sequences of PCR products were confirmed by direct sequencing.

For overlapping PCR, we used the iProof HF long PCR system (BioRad, USA). The reaction mixture contained 1× master mix, 0.2 μl each of 50-μM forward and reverse primers, and template DNA. Primers are as follows:

162F (5′-TCTGAATGCAATGTATGACTGAGATCC-3′) and
2821R (5′-ATCTGAGCTGCTGCGCCCAGGAAAGCTGG-3′) for 2659-bp PCR products;
2682F (5′-GACGCTTATGACGCTCCACTGGATGCGCAT-3′) and
6011R (5′-CTCTGCCATCTGAAGCCTCTTGCGCGTACC-3′) for 2940-bp PCR products;
5622F (5′-GGGACGTACCAGCGGAAGTACACACAATGA-3′) and
9011R (5′-TCACTCAAGCACAGGCTATGGACCAGCCCC-3′) for 3389-bp PCR products;
8382F (5′-TCAGTCATGCCGCCTGTAGAAAGCACCTG-3′) and
12011R (5′-ACGCCCCCCATGCCTGACCCTATGTTCGG-3′) for 3629-bp PCR products;
11142F (5′-GTCATACGTCCGTGCGCTGCCCTGAGGAAC-3′) and
15011R (5′-TTTATGAAGGAAGTAATATGTGTTTAATTC-3′) for 3869-bp PCR products;
371R (5′-CAAGTATGAGTCATTTCAATTGTATGAGCC-3′) and
14442F (5′-AGTTCTGTGACCACTGATCCCAGCTTAG-3′) for 1240-bp PCR products.

Each PCR cycle consisted of 98 °C for 30 s, followed by denaturing at 98 °C for 5 s, annealing at 55 °C for 15 s, and extension at 72 °C for 15 min. This reaction was performed for 35 cycles. The nucleic acid sequences were confirmed by direct sequencing.

For PCR with high sensitivity, we used AmpliTaq Gold Master (Applied Biosystems). The reaction mixture contained 1× master mix, 0.5 μl each of 50-μM forward and reverse primers, and template DNA. Primers are as follows (Fig. 3B):

JEECV-A1 (5′-GACGGTCCTAAACATGAACGGTGAAATGTC-3′) and
JEECV-A2 (5′-GGTATTTTGTACTCATTCATAGTGGCAATC-3′) for 270 bp as primer set A;
JEECV-B1 (5′-TGGGTGACCCCGAAGGGGCACTGTACG-3′) and
JEECV-B2 (5′-TATGTATAAACAGATTACGTGGCATACCTG-3′) for 240 bp as primer set B; and
JEECV-C1 (5′-TGCGCCCAGGCTTACCCTGTGCTCGATGTC-3′) and
JEECV-C2 (5′-CGGGCAGACGCAGACAACGCACTGCTGAAC-3′) for 330 bp as primer set C.

Each PCR cycle consisted of activation of Taq polymerase at 95 °C for 9 min, followed by denaturing at 95 °C for 30 s, annealing at 65 °C for 30s, and extension at 72 °C for 1 min. This reaction was performed for 70 cycles. The nucleic acid sequences were confirmed by direct sequencing.

RT-PCR

RNA was extracted from JEECV- and mock-infected cells at 3 days p.i. using an Isogen RNA extraction kit (Nippon Gene, Japan). To eliminate viral DNA from the RNA solution, RNA was repurified using a Total RNA Isolation Mini Kit (Agilent Technologies Inc., USA). Furthermore, Turbo DNA free was used to digest DNA completely. cDNA was synthesized using Superscript III (Invitrogen, USA) with random primers. As a control, the reaction was performed without Superscript III enzyme. PCR was performed using primers 024-2 and 024-5 (5′-TCAGGGTGGTCTGCTTCCGG-3′) using GoTaq (30 cycles). The size of PCR products was 503 bp.

Real-time PCR

The primers and probe were designed for a segment of the large T-antigen-like region. The primers are 025-1 (5′-TTGCCGCACC-TGCTTCAG-3′) and 025-2 (5′-CGAACACCGTAATTGGAATAAAGC-3′) for a 120-bp PCR product, and the probe is 025P (5′-FAM-ACACGC-TGCTCAAATTGCTGCTGCCT-TAMRA-3′). Serial dilution of known copies of JEECV DNA as a purified PCR product (primers 024F1 and 024R1) was used as standard DNA for real-time PCR. The TaqMan real-time PCR assay was performed in a 7500 Sequence Detection System using TaqMan Gene Expression Master Mix (Applied Biosystems) according to the instruction manual. For a time-course study of viral infection, DNA was extracted from the cells and supernatant using a QIAamp DNA mini kit. Three microliters of eluted DNA (total 50 μl) from supernatant and 10-ng eluted DNA from cells were used as templates. The thermal cycling profile of this assay comprised the following steps: 2 min at 50 °C, 10 min at 95 °C, followed by 45 cycles of PCR at 95 °C with denaturing for 15 s and at 60 °C for 1 min with annealing/extension for 1 min. The TaqMan assay was performed triplicate for each sample. DNA standards (copy number: 1 to 1×10^7) were used to construct a standard curve.

Southern blot analysis

Frozen cell pellets of virus-infected and uninfected cells were thawed and resuspended in 200-μl PBS (−). The samples were then frozen and thawed two more times followed by centrifugation with 13,000*g* at 4 °C for 10 min to produce pellets. The supernatant, approximately 200 μl, was extracted for DNA using the QIAamp MiniElute virus spin kit (Qiagen), and the extracted DNA was resuspended in 100 μl of buffer AVE. DNA (1.7 μg) was digested

using *BglII* for 4 h or not digested and run in 0.8% agarose gels. The probe used was the gel-purified PCR product using 2682F and 6011R primers, and the Megaprime DNA Labeling System (GE Healthcare) was used for ^{32}P-labeling. Hybridization was performed in ULTRAhyb (Ambion) with labeled probe at 42 °C for 15 h. Membrane washing was performed six times under the condition of 0.1× SSC and 0.1% SDS at 42 °C for 15 min. The signal was detected using X-ray film and Image analyzer (FLA2000, Fuji film, Japan).

Analysis using next generation sequencer

Viral DNA was extracted using a QIAamp DNA mini kit after precipitation using ultracentrifugation of 30-ml virus-infected supernatant (T-75 flask; Falcon) at 4 days p.i. The viral DNA was randomly amplified using Genomiphi V2 (GE Healthcare, USA) containing Phi29 enzyme, and single-stranded DNA was digested using S1 nuclease. The Genome Sequencer FLX System (Roche and 454 Life Sciences) was used in this study. DNA sequencing libraries were constructed and sequenced using Hokkaido System Science Ltd. The total number of reads was 17,000, and the total number of bases was 5,146,764. The read sequences were analyzed using GS *De novo* Assembler Version 2.3 (Roche) for *de novo* assembly.

Alignment of amino acid sequences

Nucleic acid sequences of JEECV were analyzed using BLASTx at NCBI. The polyomavirus large T-antigen-like region of JEECV was compared with that of polyomaviruses deposited in GenBank. Alignment was performed using MEGA4 software.

Acknowledgments

We thank Ms. Momoko Ogata of the National Institute of Infectious Diseases of Japan for her assistance. This study was supported in part by a grant from the Ministry of Education, Culture, Sports, Science, and Technology, Japan (#21580235 Scientific Research C:general). We are very grateful to the advice of Dr. Hiritaka Konuma, Tokai University, Drs. Hirokazu Kimura and Haruo Watanabe, National Institute of Infectious Diseases.

References

Bennett, M.D., Woolford, L., Stevens, H., Van Ranst, M., Oldfield, T., Slaven, M., O'Hara, A.J., Warren, K.S., Nicholls, P.K., 2008. Genomic characterization of a novel virus found in papillomatous lesions from a southern brown bandicoot (Isoodon obesulus) in Western Australia. Virology 376, 173–182.

Bennett, M.D., Reiss, A., Stevens, H., Heylen, E., Van Ranst, M., Wayne, A., Slaven, M., Mills, J.N., Warren, K.S., O'Hara, A.J., Nicholls, P.K., 2010. The first complete papillomavirus genome characterized from a marsupial host: a novel isolate from *Bettongia penicillata*. J. Virol. 84, 5448–5453.

Egusa, S., Tanaka, M., Ogami, H., Oka, H., 1989. Histopathological observations on an intense congestion of the gills in cultured Japanese eel, *Anguilla japonica*. Fish Pathol. 24, 51–56.

Inoue, K., Miwa, S., Aoshima, H., Oka, H., Sorimachi, M., 1994. A histopathological study on the etiology of intense congestion of the gills of Japanese eel, *Anguilla japonica*. Fish Pathol. 29, 35–41.

John, R., Muller, H., 2007. Polyomaviruses of birds: etiologic agents of inflammatory diseases in a tumor virus family. J. Virol. 81, 11554–11559.

Johne, R., Muller, H., Rector, A., van Ranst, M., Stevens, H., 2009. Rolling-circle amplification of viral DNA genomes using phi29 polymerase. Trends Microbiol. 17, 205–211.

Maeda, K., Hondo, E., Terakawa, J., Kiso, Y., Nakaichi, M., Endoh, D., Sakai, K., Morikawa, S., Mizutani, T., 2008. Isolation of a novel adenovirus from a fruit bat (*Pteropus dasymallus yayeyamae*). Emerg. Infec. Dis. 14, 347–349.

Mills, R., Rozanov, M., Lomsadze, A., Tatusova, T., Borodovsky, M., 2003. Improving gene annotation in complete viral genomes. Nucleic Acids Res. 31, 7041–7055.

Mizutani, T., Endoh, D., Okamoto, M., Shirato, K., Shimizu, H., Arita, M., Fukushi, S., Saijo, M., Sakai, K., Limn, C.K., Ito, M., Nerome, R., Takasaki, T., Ishii, K., Suzuki, T., Kurane, I., Morikawa, S., Nishimura, H., 2007. Rapid genome sequencing of RNA viruses. Emerg. Infec. Dis. 13, 322–324.

Ono, S., Nagai, A., 1997. Electronmicroscopic observation and experimental infection of congestion in gills of Japanese eel, *Anguilla japonica*. J. School Marine Sci. Technol. 43, 95–105.

Ono, S., Wakabayashi, K., Nagai, A., 2007. Isolation of the virus causing viral endothelial cell necrosis of eel from cultured Japanese eel, *Anguilla japonica*. Fish Pathol. 42, 191–200.

Pipas, J.M., 1992. Common and unique features of T antigens encoded by the polyomavirus group. J. Virol. 66, 3979–3985.

Sakai, K., Ueno, Y., Ueda, S., Yada, K., Fukushi, S., Saijo, M., Kurane, I., Mutoh, K., Yoshioka, K., Nakamura, M., Takehara, K., Morikawa, S., Mizutani, T., 2009. Novel reovirus isolation from an Ostrich (*Struthio camelus*) in Japan. Vet. Microbiol. 134, 227–232.

Tanaka, M., Satoh, T., Ma, W.J., Ono, S., 2008. Effectiveness of increasing temperature of rearing water and non-feeding against viral endothelial cell necrosis of eel. Fish Pathol. 43, 79–82.

Watanabe, S., Maeda, K., Suzuki, K., Ueda, N., Iha, K., Taniguchi, S., Shimoda, H., Kato, K., Yoshikawa, Y., Morikawa, S., Kurane, I., Akashi, H., (in press). Identification of a novel betaherpesvirus in bats using a rapid determination system for viral RNA sequences (RDV). Emerg. Infect. Dis.

Watanabe, S., Ueda, N., Iha, K., Masangkay, J.S., Fujii, H., Alviola, P., Mizutani, T., Maeda, K., Yamane, D., Walid, A., Kato, K., Kyuwa, S., Tohya, Y., Yoshikawa, Y., Akashi, H., 2009. Detection of a new bat gammaherpesvirus in the Philippines. Virus Genes 39, 90–93.

Woolford, L., Rector, A., Van Ranst, M., Ducki, A., Bennett, M.D., Nicholls, P.K., Warren, K. S., Swan, R.A., Wilcox, G.E., O'Hara, A.J., 2007. A novel virus detected in papillomas and carcinomas of the endangered western barred bandicoot (*Perameles bougainville*) exhibits genomic features of both the Papillomaviridae and Polyomaviridae. J. Virol. 81, 13280–13290.

Woolford, L., O'Hara, A.J., Bennett, M.D., Slaven, M., Swan, R., Friend, J.A., Ducki, A., Sims, C., Hill, S., Nicholls, P.K., Warren, K.S., 2008. Cutaneous papillomatosis and carcinomatosis in the Western barred bandicoot (*Perameles bougainville*). Vet. Pathol. 45, 95–103.

Woolford, L., Bennett, M.D., Sims, C., Thomas, N., Friend, J.A., Nicholls, P.K., Warren, K.S., O'Hara, A.J., 2009. Prevalence, emergence, and factors associated with a viral papillomatosis and carcinomatosis syndrome in wild, reintroduced, and captive western barred bandicoots (*Perameles bougainville*). EcoHealth 6, 414–425.

Yamao, T., Eshita, Y., Kihara, Y., Satho, T., Kuroda, M., Sekizuka, T., Nishimura, M., Sakai, K., Watanabe, S., Akashi, H., Rongsriyam, Y., Komalamisra, N., Srisawat, R., Miyata, T., Sakata, A., Hosokawa, M., Nakashima, M., Kashige, N., Miake, F., Fukushi, S., Nakauchi, M., Saijo, M., Kurane, I., Morikawa, S., Mizutani, T., 2009. Novel virus discovery from field-collected mosquito larvae using an improved system for rapid determination of viral RNA sequences (RDV ver4.0). Arch. Virol. 154, 153–158.

Cell PRESS

Chemistry & Biology
Article

Natural Product-Like Macrocyclic *N*-Methyl-Peptide Inhibitors against a Ubiquitin Ligase Uncovered from a Ribosome-Expressed De Novo Library

Yusuke Yamagishi,[1] Ikuo Shoji,[2] Shoji Miyagawa,[2] Takashi Kawakami,[1] Takayuki Katoh,[3] Yuki Goto,[3] and Hiroaki Suga[3,*]
[1]Department of Chemistry and Biotechnology, Graduate School of Engineering, The University of Tokyo, 7-3-1 Hongo, Bunkyo-ku, Tokyo 113-8656, Japan
[2]Division of Microbiology, Center for Infectious Diseases, Kobe University Graduate School of Medicine, 7-5-1 Kusunoki-cho, Chuo-ku, Kobe, Hyogo 650-0017, Japan
[3]Department of Chemistry, Graduate School of Science, The University of Tokyo, 7-3-1 Hongo, Bunkyo-ku, Tokyo 113-0033, Japan
*Correspondence: hsuga@chem.s.u-tokyo.ac.jp
DOI 10.1016/j.chembiol.2011.09.013

SUMMARY

Naturally occurring peptides often possess macrocyclic and *N*-methylated backbone. These features grant them structural rigidity, high affinity to targets, proteolytic resistance, and occasionally membrane permeability. Because such peptides are produced by either nonribosomal peptide synthetases or enzymatic posttranslational modifications, it is yet a formidable challenge in degenerating sequence or length and preparing libraries for screening bioactive molecules. Here, we report a new means of synthesizing a de novo library of "natural product-like" macrocyclic *N*-methyl-peptides using translation machinery under the reprogrammed genetic code, which is coupled with an in vitro display technique, referred to as RaPID (random nonstandard peptides integrated discovery) system. This system allows for rapid selection of strong binders against an arbitrarily chosen therapeutic target. Here, we have demonstrated the selection of anti-E6AP macrocyclic *N*-methyl-peptides, one of which strongly inhibits polyubiqutination of proteins such as p53.

INTRODUCTION

Peptides discovered as natural products share structural features that are not seen in ordinary polypeptides (proteins) expressed by the translation apparatus. Such "nonstandard" peptides are often macrocyclized and *N*-methylated in the backbone (Chatterjee et al., 2008); moreover, some of their side chains are modified to noncanonical functional groups or epimerized to *D*-configuration (Grünewald and Marahiel, 2006; Kohli et al., 2002; Li and Roller, 2002). These features concede critical biological and pharmacological properties, such as high affinity to binding partners, proteolytic resistance, and membrane permeability, and thus increase their specific potencies in vivo (Biron et al., 2008; Doedens et al., 2010; Driggers et al., 2008; Nestor, 2009; Sagan et al., 2004). Most of these peptides are produced by nonribosomal peptide synthetases (Grünewald and Marahiel, 2006; Kohli et al., 2002; Li and Roller, 2002) or are derived from ribosomally expressed peptides by enzymatic posttranslational modifications (Chatterjee et al., 2005; McIntosh et al., 2009; Oman and van der Donk, 2010). Despite the fact that libraries of "natural product-like" nonstandard peptides could be a very attractive source for drug discovery campaigns, the mechanistic and functional complexities of their production systems have been making it difficult for researchers to degenerate the sequences and lengths of nonstandard peptides and build their de novo library. Therefore, we have not yet witnessed a successful outcome of the generation of a highly complex "human-made" library and the discovery of novel peptide sequences against therapeutic targets.

Here, we report a unique means of synthesizing a "natural product-like" peptide library using a custom-made translation apparatus under the reprogrammed genetic code. The peptides in the library have the features of macrocyclic and *N*-methylated backbone along with a *D*-amino acid involvement in the sequences. Moreover, the library could be coupled with an in vitro display, and thus over a trillion members of nonstandard peptides can be rapidly screened against a chosen target. We referred to this platform system as RaPID (random nonstandard peptides integrated discovery) system. As a showcase of this system, we have performed selection of anti-E6AP macrocyclic *N*-methyl-peptides, and one of the abundant classes of selected peptides exhibited an inhibitory activity against E6AP-catalyzed polyubiquitination of target proteins, such as p53 and peroxiredoxin 1. Thus, the present work demonstrates a proof-of-technology and potentials of the RaPID system for the discovery of a novel class of nonstandard peptides against not only an E3 Ubquitin ligase but also previously nondruggable target families.

RESULTS AND DISCUSSION

Design of a Nonstandard Peptide Library Used in the RaPID System

The methodology of genetic code reprogramming, where arbitrary codons are reassigned from proteinogenic amino acids to nonproteinogenic amino acids, allows us to express "nonstandard" peptides using a translation apparatus (Forster et al., 2003; Josephson et al., 2005; Ohta et al., 2007; Ohta et al., 2008). To facilitate such a reprogramming, we have

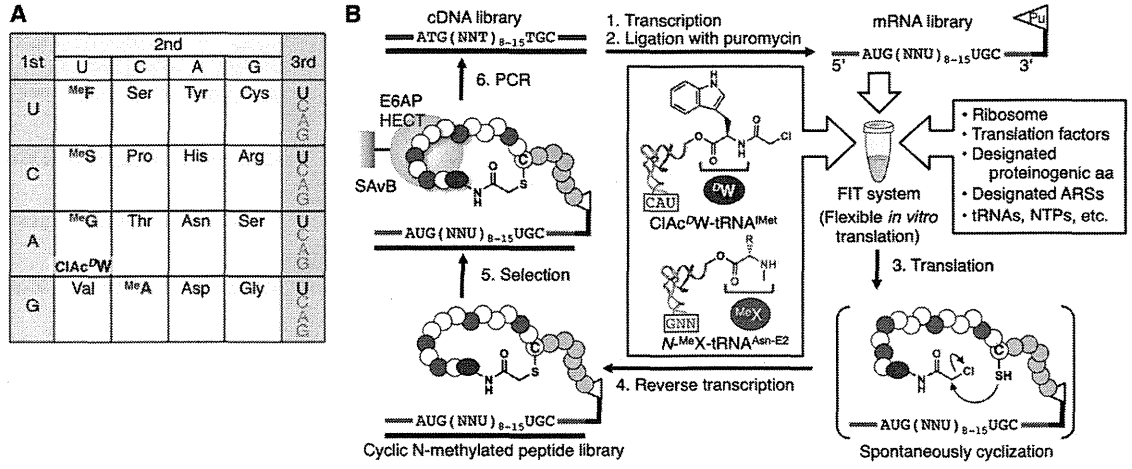

Figure 1. In Vitro Selection of Macrocyclic *N*-Methylated Peptides against E6AP HECT Domain by RaPID System

(A) The genetic code reprogrammed for this study. Four *N*-methyl-amino acids (^{Me}F, ^{Me}S, ^{Me}A, and ^{Me}G) and chloroacetyl-*D*-tryptophan (ClAc^{D}W) are shown in red and blue, respectively.

(B) Overview of the RaPID system for the selection of macrocyclic *N*-methyl-peptides. Messenger RNA libraries containing random sequence domain, $(NNU)_{8-15}$, were transcribed from the corresponding cDNA library and were conjugated with an oligonucleotide bearing a 3′-puromycin residue. The resulting mRNAs were translated by FIT system in the presence of the appropriate aminoacyl-tRNAs prepared by flexizymes. Linear peptides displayed on the individual mRNAs were spontaneously cyclized after translation, and the resulting macrocyclic peptides are displayed. The peptide libraries were then subjected to biotin-Avi-$(His)_6$-GB1-HECT immobilized on streptavidin magnetic beads (SAvB), and active species are isolated. Reverse transcription was performed after the selection in the first round and before the selection from the second round. The cDNAs on active mRNA-peptide fusion were recovered and amplified by PCR.

developed the FIT (flexible in-vitro translation) system (Goto et al., 2011). This system involves a custom-made *Escherichia coli* reconstituted cell-free translation system (Kung et al., 1977; Shimizu et al., 2001), where arbitrary amino acids and cognate aminoacyl-tRNA synthetases (ARSs) can be omitted to make the corresponding codons vacant, to which nonproteinogenic amino acids are assigned by supplementing the corresponding aminoacyl-tRNAs prepared by the flexizyme (flexible tRNA acylation ribozyme) technology (Murakami et al., 2006; Ohuchi et al., 2007). In fact, by using a customized FIT system, we were able to express macrocyclic *N*-methyl-peptides under the genetic code reprogrammed with more than four kinds of *N*-methyl-amino acids (Kawakami et al., 2008). To construct highly diverse libraries of nonstandard peptides and to effectively screen them for designated bioactivity, the FIT system was further integrated with an in vitro display method, so-called mRNA display (Nemoto et al., 1997; Roberts and Szostak, 1997). By this integration, nonstandard peptides expressed by the FIT system would be covalently ligated to the respective mRNAs via puromycin, displaying nonstandard peptides for the desired activity panning. We referred this mRNA display system integrated with FIT system to as RaPID (random nonstandard peptides integrated discovery) system.

In the present work, we assigned five nonproteinogenic amino acids, *N*-(2-chloroacetyl)-*D*-tryptophan (ClAc^{D}W), *N*-methylphenylalanine (^{Me}F), *N*-methylserine (^{Me}S), *N*-methylglycine (^{Me}G), and *N*-methylalanine (^{Me}A), to AUG, UUU, CUU, AUU, and GCU codons by the addition of ClAc^{D}W-tRNA$^{fMet}_{CAU}$, ^{Me}F-tRNA$^{Asn\text{-}E2}_{GAA}$, ^{Me}S-tRNA$^{Asn\text{-}E2}_{GAG}$, ^{Me}G-tRNA$^{Asn\text{-}E2}_{GAU}$, and ^{Me}A-tRNA$^{Asn\text{-}E2}_{GGC}$, respectively, prepared by the flexizyme technology (Figure 1A). A mRNA library was constructed to have NNU codon (N represents any of four bases, A, G, C, and U) with the mixture of repeats from eight to 15, $(NNU)_{8-15}$; thereby, *N*-methyl-amino acids would randomly appear in this region with the lengths of eight to 15 residues. In right downstream of the random region, UGC that assigns cysteine (Cys) was installed. Because all expressed peptides should have a ClAc^{D}W at the N terminus assigned by AUG start codon, the ClAc group would intramolecularly react with the sulfhydryl group of the Cys residue assigned by UGC or potentially UGU appeared in the random region, macrocyclizing their backbone via a nonreducible thioether bond (Goto et al., 2008; Kawakami et al., 2008). Following the UGC codon, three repeats of (GGC)(AGC) encoding $(Gly\text{-}Ser)_3$ followed by UAG stop codon are embedded. The 3′ common sequence would facilitate the display of macrocyclic *N*-methyl-peptides on the respective mRNA molecules via the $(Gly\text{-}Ser)_3$-puromycin linkage (Figure 1B).

Three critical notes should be given for securing a high quality of the macrocyclic *N*-methyl-peptide library: (1) In this FIT system, the amino acids and their cognate ARSs, whose codons were reprogrammed (F, L, I, and A), were omitted from the translation components, minimizing the unwanted incorporation of these proteinogenic amino acids competing with the *N*-methyl-amino acids. Similarly, those unassigned by NNU codons (Q, K, E, and W) were omitted. Moreover, release factor-1 (RF1) was withdrawn to aim at halting elongation at UAG codon and thus increasing the efficiency of puromycin-peptide fusion. (2) Because four of 16 codons assigned by the NNU mRNA library encode *N*-methyl-amino acids, one *N*-methyl-amino acid residue would appear in every four residues by chance. Our previous studies suggested the thioether macrocyclization takes place cleanly in nearly quantitative manner, regardless of the length and composition of peptide

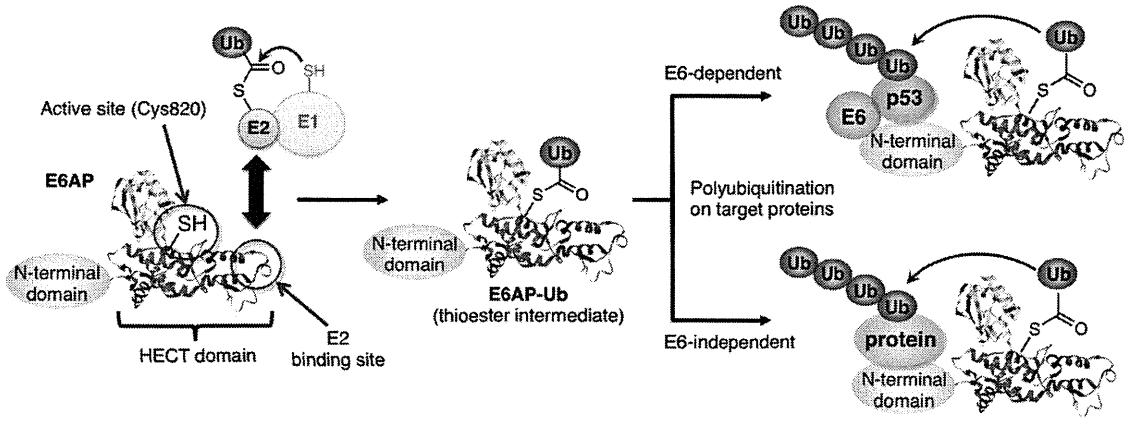

Figure 2. E6AP-Catalyzing Polyubiqutination of Target Proteins in E6-Independent and -Dependent Manners
In general, ubiquitin-activating enzyme E1 delivers an ubiquitin molecule (Ub) onto ubiquitin-conjugating enzyme E2 via a thioester linkage, and then Ub on E2 is transferred to ubiquitin ligase E3 forming a conjugate, E3-Ub. E6AP HECT (homologous to E6-associated protein [E6AP] C-terminus) domain (PDB 1C4Z), belonging to a member of E3 protein family, cooperatively catalyzes polyubiquitination on certain proteins, such as p53, with E6 (E6-dependent pathway) or directly polyubiquitinates various target proteins (E6-indendent pathway).

sequences (Goto et al., 2008; Kawakami et al., 2008). Moreover, because no stop codon was encoded in the $(NNU)_{8-15}$ random region, the highly reliable macrocyclic *N*-methyl-peptide library could be displayed by RaPID system. (3) The initial mRNA library consists of greater than 6×10^{12} unique members. It should be noted that the complexity of $(NNU)_{8-15}$ mRNA library should almost directly reflect to the peptide library complexity because only Ser is redundant in the genetic triplets used. Because the generally observed yield of mRNA-peptide fusion in the FIT system was 30% or more of the total input of mRNA, the diversity of the initial RaPID display library was estimated to be 10^{12} or more.

RaPID Selection against E6AP HECT Domain

The ubiquitin-proteasome system regulates the degradation of cellular proteins through enzyme cascade consisting of ubiquitin-activating enzyme E1, ubiquitin-conjugating enzyme E2, and ubiquitin (Ub) ligase E3 (Figure 2) (Hershko and Ciechanover, 1998; Pickart, 2001). Many families of E3 Ub ligases are known and are responsible for specific conjugation of polyubiquitins (polyUbs) to designated proteins, directing them to proteasome and thus triggering their proteolysis. Misregulation of the proteolysis of certain proteins caused by malfunction of E3 family ligases influences their downstream signal transduction processes, and therefore causes human disorders such as cancer (Hoeller et al., 2006) and neurodegeneration (Layfield et al., 2005; Rubinsztein, 2006). Thus, these E3 Ub ligases could be attractive targets for new therapeutic intervention (Eldridge and O'Brien, 2010; Hoeller and Dikic, 2009; Nalepa et al., 2006). Homologous to E6AP C-terminus (HECT) domain belongs to a family member of E3, and its N terminus domain cooperates with the human papillomavirus (HPV) E6 protein originating from the high-risk virus types 16 and 18 (Beaudenon and Huibregtse, 2008; Scheffner et al., 1993). The resulting E6AP and E6 complex provides the specific E3 ligase activity in the transfer of polyUbs onto p53 for the promotion of degradation, inhibiting p53-dependent apoptosis pathways (Figure 2). Moreover, it has been discovered that E6AP ubiquitinates some endogenous human proteins, such as HHR23A (a human homolog of the yeast DNA repair protein Rad23) (Kumar et al., 1999) and PML (promyelocytic leukemia) tumor suppressor (Louria-Hayon et al., 2009), in an E6-independent manner, suggesting that it also promotes the degradation of tumor-associated proteins. Despite advances in understanding of the molecular mechanism and structural study for HECT domains of E6AP (Huang et al., 1999) and other related enzymes (Eletr and Kuhlman, 2007; Ogunjimi et al., 2005), to the best of our knowledge, no selective inhibitor against E6AP has been yet reported by means of high-throughput screenings. Therefore, the development of inhibitors against HECT domain remains a formidable challenge. We here chose E6AP as a previously nondruggable target and performed selection of anti-E6AP peptides using RaPID system.

E6AP HECT domain was expressed as a fusion protein with an Avi-$(His)_6$-tag followed by a solubility-enhancement tag GB1 (streptococcal B1 immunoglobulin-binding domain of protein G) (Liu et al., 2009; Zhou et al., 2001) at the N terminus. This protein construct, Avi-$(His)_6$-GB1-HECT, in which Avi domain was biotinylated during the expression, was immobilized on streptavidin magnetic beads (SAvB, Figure 1B). The library was applied to the protein beads, and the bound fractions were selected at 4°C in the first and second round (Figure 3A). From the third round, GB1-immobilized SAvB was used as the negative selection to remove GB1-binding peptides, and then the positive selection was performed at 37°C to enrich the population with specific binding activity against the HECT domain. In the sixth round, we observed a significant increase in recovery rate of active fractions (Figure 3A), and therefore the resulting cDNA sequences in the pool were analyzed.

The sequence alignment of 47 clones revealed eight independent sequence families found in the pool 6 (Figure 3B). Six families, CM_{11}-1–6, are originating from the $(NNU)_{11}$ pool, whereas the remaining two families, CM_{13}-7 and CM_{13}-8, are from the $(NNU)_{13}$ pool. The most abundant sequence, CM_{11}-1, bearing four *N*-methyl residues, shares several common signatures of

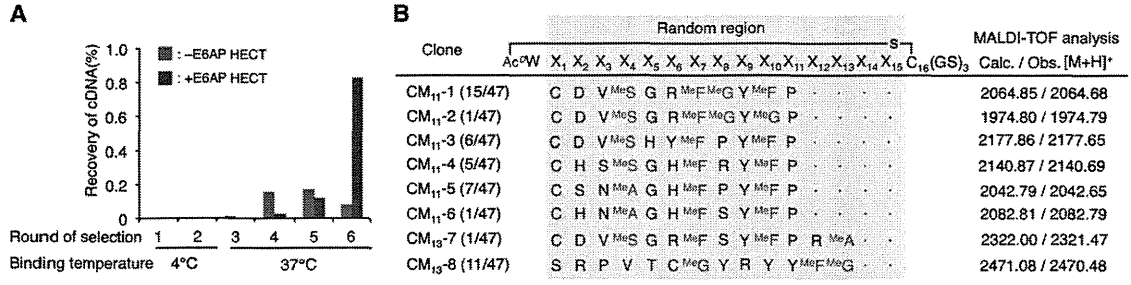

Figure 3. In Vitro Selection of Macrocyclic *N*-Methyl-Peptides against E6AP HECT Domain and Selected Active Species

(A) Progress of the selection. Recovery rates of cDNA from each round were estimated by recovered amounts over input amounts of cDNAs monitored by real-time PCR. The first and second rounds of selection were performed at 4°C, and the subsequent rounds were performed at 37°C. Those determined against SAvB•biotin-Avi-$(His)_6$-GB1-HECT as a positive selection are shown in blue, whereas those against SAvB•biotin-Avi-$(His)_6$-GB1 as a negative selection shown in red.

(B) Peptide sequences identified from the pool in round 6. The apparent frequency over a total number of clones and *N*-methyl amino acids of each sequence are shown in parentheses and red, respectively. The parental random region is highlighted in gray, in which a dot denotes a residue that did not appear in the random X_{12-15} region. Calculated (Calc.) and observed (Obs.) mass values ($[M+H]^+$) of each peptide expressed by FIT system are shown. See also Figure S1 and Table S1.

residues with other sequences. $^{Me}S_4$, G_5, $^{Me}F_7$, Y_9, $^{Me}F_{10}$, and P_{11} are highly conserved in CM_{11}-1–6 and CM_{13}-7, where four residues are notably the secondary amino acids. Among them, $^{Me}F_{10} \rightarrow {}^{Me}G_{10}$ as well as $^{Me}S_4 \rightarrow {}^{Me}A_4$ substitutions were found in CM_{11}-2 and CM_{11}-5/CM_{11}-6, respectively, suggesting that the role of side chain group may be less important in activity but critical to be the *N*-methyl substituent. Moreover, $^{Me}G_8$ could be substituted with P_8 observed in abundant CM_{11}-3 and CM_{11}-5, whereas another abundant CM_{11}-4 and two other independent peptides CM_{11}-6–7 have R_8 and S_8, respectively. This may suggest that X_8 prefers to be the secondary amino acid but tolerates other amino acid substitutions. Mutations occurred during the course of selection is discussed more details in the Supplemental Information (see Figure S1 available online).

It is intriguing that the selection yielded only two lengths of *N*-methyl-peptides from the $(NNU)_{8-15}$ random region, given that other lengths of peptides should coexist in the initial pool, suggesting that the three-dimensional structure arisen from these two lengths might be critical to exhibit binding activity against E6AP HECT domain (Figure 3B). Importantly, the successful outcomes clearly demonstrated that the *N*-methyl-peptide library used in this study had a reliable quality and high complexity giving the *N*-methyl residues in the random region, and the RaPID system enabled us to select active species effectively and rapidly. The observed similarity in the composition of amino acid residues, particularly the positions as well as kinds of *N*-methyl residues appeared in the sequences, also suggests that specific interactions between the selected *N*-methyl-peptides and E6AP HECT domain are very likely occurring.

Characterization of Isolated Anti-E6AP Macrocyclic *N*-Methyl-Peptides

To confirm whether the identified mRNA sequences of CM_{11}-1–6 and CM_{13}-7–8 correctly produced the encoding macrocyclic *N*-methyl-peptides, we constructed the respective mRNA templates with a substitution of UAG with UAA that acts as a terminator of endogenous RF2 and performed in vitro expression using the same FIT system as the selection (Figure 3B, data in the column of MALDI-TOF analysis). MALDI-TOF analysis of the crude product expressed from the respective mRNA template showed a clean peak of which molecular mass is consistent with that calculated. This observation made us confident that the selected peptides had the *N*-methylated backbone as well as the composition of residues, as we expected from the cDNA sequences. For further characterization, we decided to focus on three abundant peptides, CM_{11}-1, CM_{11}-3, and CM_{11}-5, all of which consist of a total of 14 amino acid residues. The respective *N*-methyl-peptides were chemically synthesized by standard Fmoc solid-phase chemistry where the C terminus of G_{17} (corresponding to the 14th residue) was modified with carboxyamide (Table S1).

Because the above three peptides have a cysteine residue at position 1 (C_1) in the random region adjacent to $ClAc^DW$, cyclization between the ClAc group with C_1 side chain designated by UGU would potentially compete with that between the ClAc group with C_{16} side chain designated by UGC. To decipher which cyclization preferentially or selectively occurred, we synthesized three peptides based on CM_{11}-1 as a representative peptide; one is CM_{11}-1 itself, and the others are $C_1 \rightarrow S_1$ mutant of CM_{11}-1 (CM_{11}-$1S_1$) and the corresponding to linear *N*-methyl-peptide by altering ClAc to acetyl (Ac) group, referred to as LM_{11}-1 (Table 1). Fragmentation of LM_{11}-1 by MALDI-TOF/TOF yielded peaks corresponding to linear fragments, as expected (Figure S2A). On the other hand, MALDI-TOF/TOF fragmentation of CM_{11}-1 and CM_{11}-$1S_1$ was much difficult than that for LM_{11}-1, and both gave similar fragmentation patterns (Figures S2B and S2C). Importantly, we were able to identify peaks corresponding to fragments containing the thioether linkage between the N-terminal acetyl group and the sulfhydryl group of C_{16} side chain in both CM_{11}-1 and CM_{11}-$1S_1$, but not between Ac and C_1 side chain in CM_{11}-1. These results well agree with the selective formation of the thioether linkage of Ac-S-C_{16}.

To evaluate the binding abilities of chosen peptides, CM_{11}-1, CM_{11}-3, and CM_{11}-5 (a series of these peptides are referred to as CM_{11}-peptides), we determined their kinetic and dissociation constants by means of surface plasmon resonance (SPR)

Table 1. Kinetic and Equilibrium Constants of Macrocyclic *N*-Methyl-Peptides against E6AP HECT Domain

Peptide	Sequence	k_{on} (x10^6) M^{-1}s^{-1}	k_{off} (x10^{-3}) s^{-1}	K_d nM
CM_{11}-1	$Ac^{D}WCDV^{Me}SGR^{Me}F^{Me}GY^{Me}FPCG\text{-}NH_2$ (S–C$_{16}$)	2.66	1.60	0.60
LM_{11}-1	$Ac^{D}WCDV^{Me}SGR^{Me}F^{Me}GY^{Me}FPCG\text{-}NH_2$	0.047	8.46	180
CM_{11}-1S_1	$Ac^{D}WSDV^{Me}SGR^{Me}F^{Me}GY^{Me}FPCG\text{-}NH_2$ (S–C$_{16}$)	1.33	15.5	11.7
CP_{11}-1	$Ac^{D}WCDV\ S\ GR\ F\ G\ \ Y\ F\ PCG\text{-}NH_2$ (S–C$_{16}$)	not detectable		>1000
LP_{11}-1	$Ac^{D}WCDV\ S\ GR\ F\ G\ \ Y\ F\ PCG\text{-}NH_2$	not detectable		>1000
CM_{11}-3	$Ac^{D}WCDV^{Me}SHY^{Me}F\ P\ Y\ ^{Me}FPCG\text{-}NH_2$ (S–C$_{16}$)	0.257	0.320	1.24
LM_{11}-3	$Ac^{D}WCDV^{Me}SHY^{Me}F\ P\ Y^{Me}FPCG\text{-}NH_2$	0.014	4.46	325
CM_{11}-5	$Ac^{D}WCSN^{Me}AGH^{Me}F\ P\ Y^{Me}FPCG\text{-}NH_2$ (S–C$_{16}$)	2.19	2.87	1.31
LM_{11}-5	$Ac^{D}WCSN^{Me}AGH^{Me}F\ P\ Y^{Me}FPCG\text{-}NH_2$	0.089	20.6	231

Data were collected by the standard SPR method using Biocore T100 and the constants were generated by the equipped data fitting program. See also Figures S2 and S3.

analysis against the E6AP Avi-$(His)_6$-GB1-HECT domain immobilized on a SAv-sensor chip (Table 1). All macrocyclic CM_{11}-peptides have values of k_{on} with a range of 0.2–3 × 10^6 $M^{-1}s^{-1}$, k_{off} with a range of 0.3–3 × 10^{-3} s^{-1}, resulting in the dissociation constants (K_d) with subnanomolar to 1 nM range. Thus, the representative CM_{11}-peptides studied here have remarkably strong affinity to E6AP HECT domain, and particularly CM_{11}-1 has the lowest K_d values among the CM_{11}-peptides. In addition to the CM_{11}-peptides, we synthesized the respective linear peptides bearing N-terminal acetyl group, referred to as LM_{11}-peptides. All LM_{11}-peptides lost affinity over 170-fold. This suggests that the macrocyclic structure closed by the Ac-S-C_{16} thioether bond in CM_{11}-peptides is crucial to exhibit high binding activity to the HECT domain.

In addition to the above peptides, we synthesized three more mutants of CM_{11}-1 to further validate the importance of the specific structure. One was the aforementioned $C_1 \rightarrow S_1$ mutant peptide, CM_{11}-1S_1, and the others are a macrocyclic peptide without N-methyl backbone but having the same side chains, CP_{11}-1, and its linear peptide, LP_{11}-1 (Table 1). CM_{11}-1S_1 had a 9-fold faster k_{off} rate than CM_{11}-1, implying that C_1 somehow contributes to slowing the dissociation from the target site but is not absolutely essential for binding activity. On the other hand, the other two mutants completely lost binding ability, indicating that *N*-methylated backbone with the N-terminal Ac-C_{16} thioether macrocycle is crucial to maintain the full binding capability of CM_{11}-1 against E6AP HECT domain.

Furthermore, we verified the binding specificity of CM_{11}-peptides against E6AP HECT domain using a different HECT-type E3 Ub ligase, Smurf2 (Ogunjimi et al., 2005). None of CM_{11}-peptides had any SPR signature of binding against Smurf2 Avi-$(His)_6$-GB1-HECT domain immobilized on a SAv-sensor chip, indicating that CM_{11}-peptides have high selectivity toward the E6AP HECT domain over Smurf2 HECT domain nor Avi-$(His)_6$-GB1-tag region (data not shown). Moreover, we investigated human plasma stability of CM_{11}-peptides compared with other control peptides (see more details in Supplemental Information and Figure S3), indicating that a CM_{11}-peptide (CM_{11}-1S_1) is very stable in plasma. Taken together, CM_{11}-peptides have remarkable binding activity and specificity to E6AP HECT domain and plasma stability.

CM_{11}-1 Inhibits Ubiquitination of Target Proteins Catalyzed by E6AP

Despite the observation of strong binding activity of CM_{11}-peptides to E6AP HECT domain, it does not necessarily mean that they are able to inhibit the E6AP ubiquitination activity. To assess whether CM_{11}-peptides have an ability to inhibit the ubiquitination activity, we chose the most active CM_{11}-1 and performed an in vitro assay to monitor ubiquitin thioester formation. It is known that E6AP or even its HECT domain alone forms the ubiquitin thioester intermediate (Beaudenon et al., 2005; Scheffner et al., 1990; Scheffner et al., 1995) in the presence of Ub, E1, and E2 in vitro (Figure 2). When an in vitro translation system from rabbit reticulocyte lysate (RRL), which contains these essential Ub-related components, was used for translating the E6AP HECT domain from the appropriate mRNA template in the presence of [^{35}S]-Met (Huibregtse et al., 1995),

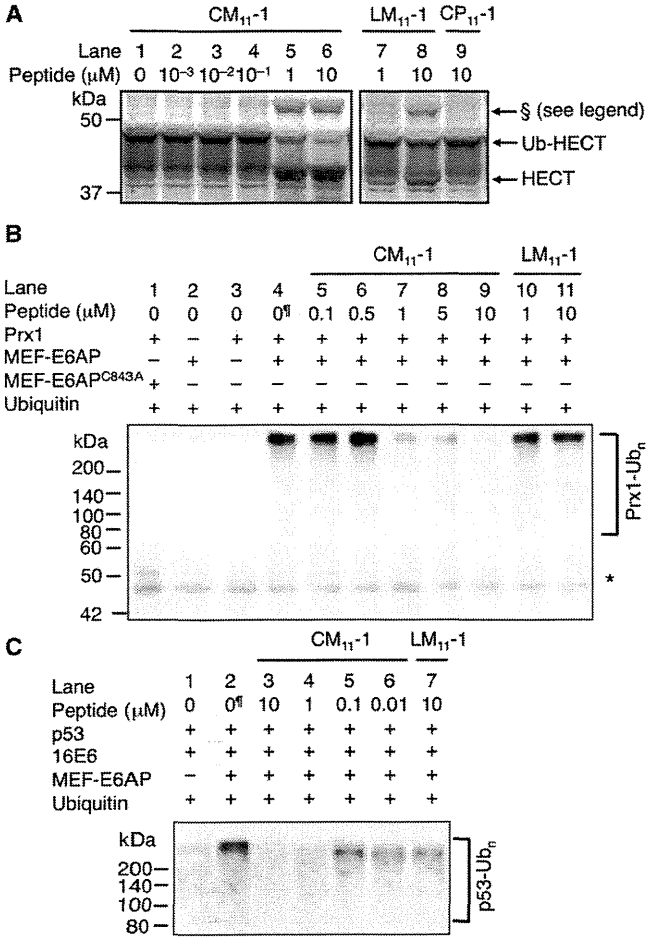

Figure 4. Inhibition of Ub-Thioester Formation with E6AP HECT Domain and Polyubiqutination of Target Proteins by CM_{11}-1 and Its Derivatives

(A) Inhibition of Ub-thioester formation with E6AP HECT domain. ^{35}S-labeled E6AP HECT (43 kDa) was translated in a rabbit reticulocyte lysate cell-free translation system. Because the translation lysate supposedly contained ubiquitin (8 kDa), E1, and E2, the expressed E6AP HECT would be endogenously converted to the ubiquitin-adduct (E6AP HECT-Ub, 51 kDa). The translation mixture was treated with various concentrations of peptides (10^{-3}–10 μM) at room temperature for 30 min. The resulting mixtures were analyzed by SDS-PAGE without DTT. §When the Ub-thioester formation on E6AP was inhibited by CM_{11}-1 (as well as 10 μM LM_{11}-1), a slower migrating band than Ub-E6AP appeared on the gel. Although the product of this band has not yet been defined, this band disappeared upon addition of a free thiol reagent such as DTT (data not shown), suggesting a possibility of dimer formation of HECT domain via a disulfide bond. Alternatively, the free cysteine in HECT domain formed a disulfide bond with other proteins containing a free cysteine residue.

(B) Inhibition of E6-independent polyubiquitination on Prx1. $(His)_6$-Prx1 was incubated with 250 nM MEF-E6AP or inactive mutant MEF-E6AP^{C843A}, $(His)_6$-E1, $(His)_6$-UbcH7, ubiquitin and peptide at 37°C for 30 min. Reaction products were immunoprecipitated with anti-Prx1 pAb and visualized by antiubiquitin mAb immunoblotting. Asterisk denotes immunoglobulin heavy chain. ¶As a negative control, DMSO used as a cosolvent for CM_{11}-1 inhibition was added.

(C) Inhibition of E6-dependent polyubiquitination on p53. p53 was incubated with 170 nM MEF-E6AP, $(His)_6$-E1, $(His)_6$-UbcH7, ubiquitin, HPV16 E6, and peptide at 37°C for 30 min. Reaction products were immunoprecipitated with anti-p53 pAb and visualized by antiubiquitin mAb immunoblotting. See also Figure S4.

a Ub-thioester intermediate of the ^{35}S-Met-labeled HECT domain (Ub-HECT) was distinguished from the parental HECT domain by means of a SDS-PAGE mobility shift assay (Figure 4A, lane 1). When CM_{11}-1 was added to this translation assay system, the migration shift was suppressed at 1 μM or higher concentrations (lanes 5 and 6). As a negative control, LM_{11}-1 and CP_{11}-1 were also tested for the same inhibition assay, in which an approximately 50% inhibition was observed at 10 μM LM_{11}-1, whereas neither 1 μM LM_{11}-1 nor 10 μM CP_{11}-1 exhibited the inhibition. Although the observed potency by CM_{11}-1 seemed not as strong as expected from the SPR data, this could be attributed to that the RRL translation system might contain endogenous label-free E6AP (Huibregtse et al., 1991; Scheffner et al., 1993) that might interact with some fractions of CM_{11}-1, resulting in a reduction of the apparent inhibitory potency. Nevertheless, this result suggests that CM_{11}-1 is able to inhibit the charge of Ub onto the HECT domain of E6AP.

We then have further pursued testing inhibition of E6AP-catalyzed polyubiquitination on target proteins. Peroxiredoxin 1 (Prx1) is an endogenous substrate of E6AP in human cells, and its polyubiquitination occurs independently from the presence of E6 (Nasu et al., 2010). To monitor the inhibitory action of CM_{11}-1 against E6AP, we used an in vitro-reconstituted Prx1 polyubiquitination assay system, in which purified His-tagged Prx1 was incubated with E6AP tagged with MEF (Myc-TEV protease site-flag) and ubiquitin in the presence of purified His-tagged E1 and E2 (UbcH7). The resulting polyubiquitinated Prx1 (Prx1-Ub_n) and free Prx1 were immunoprecipitated by anti-Prx1 polyclonal antibodies and were immunoblotted by an anti-Ub monoclonal antibody to visualize in SDS-PAGE (Figure 4B, lanes 1–9). As negative controls, LM_{11}-1 and CP_{11}-1 were also included in this examination. Clearly, polyubiquitination of Prx1 was inhibited by CM_{11}-1 in a dose-dependent manner (lanes 5–9), where an approximately 1 μM of CM_{11}-1 nearly shut down the E6AP activity. On the other hand, neither LM_{11}-1 (lanes 10 and 11) nor CP_{11}-1 (data not shown) was able to inhibit polyubiquitination. We also tested Prx1-polyubiquitination inhibition by CM_{11}-1S_1, showing a weaker inhibitory activity than CM_{11}-1 (Figure S4); the result seemed consistent with the K_d values for both peptides observed in SPR experiments.

Finally, we examined the inhibitory activity of CM_{11}-1 against polyubiquitination on an E6-dependent substrate, p53, using a reconstituted p53 polyubiquitination assay system. Immunoprecipitation of poly- and nonubiquitinated p53 using anti-p53 pAb followed by immunobolotting using anti-Ub mAb enabled us to detect the polyUb-p53 on SDS-PAGE (Figure 4C). Again, 1 μM CM_{11}-1 was able to inhibit polyubiquitination of p53 in a dose-dependent manner (lanes 3–6), whereas the control peptide, LM_{11}-1, was not (lane 7). The result shows that CM_{11}-1 acts as an E6AP inhibitor that prevents polyubiquitination of Prx1 and p53 in E6-independent and E6-dependent manner, respectively. The trend of K_d values of CM_{11}-1 and its mutant peptides against E6AP HECT domain determined by the SPR experiments well reflected to their observed inhibitory behaviors against ubiquitination of target substrates (Table 1 and Figure 4). Because the present assay method allowed us to detect polyubiquitination instead of monoubiquitination of the substrate proteins catalyzed by an excess amount of E6AP (greater than

two orders of magnitude) over the inherent K_d value of CM_{11}-1, the observed inhibitory potency of CM_{11}-1 was only qualitatively assessed. Most importantly, CM_{11}-1 was capable of inhibiting Ub ligase activity of E6AP even though it was simply selected by binding to E6AP.

SIGNIFICANCE

Here, we have demonstrated RaPID selection of "natural product-like" peptides consisting of thioether-macrocyclic and N-methylated backbone. The selection against E6AP HECT domain has yielded such desired peptides with remarkable binding abilities, falling in a range of K_d values from a subnanomolar to a single-digit nanomolar. One of the representative peptides, CM_{11}-1, chosen for further studies has displayed inhibitory activity against E6AP-catalyzing polyubiquitination on the target proteins, Prx1 and p53. The present work provides the proof-of-technology of RaPID system that enables for the discovery of potent inhibitors against a previously nondruggable ubiquitin ligase, thus opening a wide range of possibilities in the discovery of inhibitors against other ubiquitin ligase families. Most importantly, the natural product-like macrocyclic *N*-methyl-peptides have larger interaction surfaces compared with small organic molecules, as well as elevated stability under physiological conditions compared with ordinary peptides; therefore, they would provide tremendous potentials for the development of drug leads that disrupt not only enzyme activities but also protein-protein interactions.

EXPERIMENTAL PROCEDURES

In Vitro Translation and Selection

Translation of the first round selection was performed using 100 pmol mRNA-puromycin (initial complexity is 6×10^{13}) and 150 μl of translation mixture in the presence of 3750 pmol of ClAc^{D}W-tRNA$^{fMet}_{CAU}$, ^{Me}G-tRNA$^{Asn\text{-}E2}_{GAU}$, ^{Me}A-tRNA$^{Asn\text{-}E2}_{GGC}$, ^{Me}S-tRNA$^{Asn\text{-}E2}_{GAG}$, and ^{Me}F-tRNA$^{Asn\text{-}E2}_{GAA}$ (25 μM each), at 37°C for 30 min. Subsequently, the translation mixture was incubated at room temperature for 12 min to conjugate the translated peptide with the corresponding mRNA-puromycin. This solution was incubation with 15 μl of 200 mM EDTA (pH 8.0) at 37°C for 30 min in order to dissociate ribosomes from mRNA-peptide complexes. For the first-round selection, 11 μl of E6AP HECT immobilized streptavidin magnetic beads (Dynabeads M-280, Invitrogen) was used at a concentration of 200 nM target protein, and mixed with the solution of mRNA-displayed *N*-methyl-peptides. The binding reaction was performed at 4°C for 30 min with rotation. After supernatant was removed, the bead was washed with 300 μl of cold wash buffer (100 mM Tris-HCl [pH 7.5], 300 mM NaCl, 0.05% [v/v] tween 20). To the bead was added 40 μl of RT reaction buffer (50 mM Tris-HCl [pH 8.3], 75 mM KCl, 3 mM $MgCl_2$, 10 μM DTT, 0.5 mM dNTPs, 2 μM CGS3an13.R39) containing 200 units of M-MLV reverse transcriptase (Promega) and 8 units of RNase inhibitor (Promega), and reverse transcribed at 42°C for 60 min with rotation. The selected cDNA was eluted with 360 μl of PCR buffer (10 mM Tris-HCl [pH 7.5], 50 mM KCl, 0.1% [v/v] Triton X-100, 2.5 mM $MgCl_2$, 0.25 mM dNTPs, 0.25 μM T7g10M.F48, 0.25 μM CGS3an13.R39) at 95°C for 5 min. After addition of *Taq* DNA polymerase to the eluate, the mixture was used for PCR amplification. The amplified DNA was purified by the extraction with phenol/chloroform and ethanol purification and was used for the next round of selection. Since the second round, 10 μl scale of transcription and 7.5 μl of ligation with puromycin linker were carried out. The resulting mRNA-puromycin of the second round was translated using 5 μl of the translation mixture in the presence of each 25 μM acyl-tRNAs at 37°C for 30 min, followed by incubation at room temperature for 12 min. After incubation with 1 μl of 100 mM EDTA (pH 8.0) at 37°C for 30 min, the reverse transcription of the mRNA-displayed peptides was performed by RT reaction buffer in the presence of M-MLV reverse transcriptase without RNase H activity (Promega), at 42°C for 60 min with rotation. After quenching the reaction with 1 μl of 100 mM EDTA (pH 8.0), the solution was neutralized with 1.1 μl of 0.2 M HCl. The complexes with cDNA- and mRNA-displayed peptides were subjected to 2.4 μl of the magnetic bead without target and were incubated at 4°C for 30 min for negative selection at once. Subsequently, the supernatant was mixed with 0.8 μl of the magnetic bead with E6AP HECT and was incubated with 4°C for 30 min for positive selection, followed by thrice washing with 10 μl of cold wash buffer. After addition of 100 μl of PCR buffer to the bead, the cDNA were eluted at 95°C for 5 min and amplified by *Taq* DNA polymerase. In the third round and all subsequent rounds, the all experiments were performed by a half of the reaction scale of the second round. Moreover, negative selection was performed at 4°C for 20 min at three times in the third and fourth round, and at nine times in the fifth and sixth round. On the other hand, positive selections after second round were performed by mixing with the complexes of cDNA and mRNA-displayed peptides and 200 nM E6AP HECT (not immobilized on streptavidin magnetic bead) at 37°C for 30 min, followed by pull down by streptavidin magnetic bead at 37°C for 5 min with rotation. After thrice washing with 5 μl of wash buffer at room temperature, the selected cDNA was eluted with 100 μl of PCR buffer at 95°C for 5 min. After addition of *Taq* DNA polymerase to the eluate, the mixture was used for PCR amplification. To monitor the convergence of the selection process, real-time PCR (RT-PCR) was used to quantify the amounts of input and output DNA in every round. For input cDNA, 0.25 μl aliquot of the RT mixture was diluted with 150 μl of a dilution solution (10 mM Tris-HCl [pH 8.0] and 300 mM NaCl), and 1 μl of the diluted cDNA was mixed with 19 μl of PCR buffer containing SYBR Green I (Molecular Probe) and *Taq* DNA polymerase. For output cDNA, 1 μl aliquots of the eluates from the beads of positive and negative selections were mixed with 10 μl of PCR buffer containing SYBR Green I and *Taq* DNA polymerase. The reverse transcribed $(NNU)_{10}$ mRNA mixture was serial-diluted and used for the templates as standards.

MALDI-TOF Analysis of Translated Clone Peptides

To identify the expressed cyclic *N*-methylated peptides, a 5 μl scale translation reaction was performed using FIT system with 40 nM of clone DNA, 25 μM each of ClAc^{D}W-tRNA$^{fMet}_{CAU}$, ^{Me}G-tRNA$^{Asn\text{-}E2}_{GAU}$, ^{Me}A-tRNA$^{Asn\text{-}E2}_{GGC}$, ^{Me}S-tRNA$^{Asn\text{-}E2}_{GAG}$, and ^{Me}F-tRNA$^{Asn\text{-}E2}_{GAA}$ at 37°C for 30 min. After quenching with 0.2% TFA, the crude peptide mixture was desalted with C-Tip (C18 desalting SPE, Nikkyo technos) and eluted with 80% acetonitrile and 0.5% acetic acid solution saturated with the matrix α-cyano-4-hydroxycinnamic acid (Bruker Daltonics). MALDI-TOF analysis was performed using an Autoflex TOF/TOF (Bruker Daltonics) and peptide calibration standard II (Bruker Daltonics) as external standards.

SPR Analysis of Peptides

The interaction between E6AP HECT and peptides was assessed using a BIACORE T100 instrument (GE Healthcare) equipped with research-grade streptavidin sensor chip at 25°C. Biotinylated E6AP HECT was immobilized to a surface density of approximate 1,500 response units (RU) using standard immobilization protocols (GE Healthcare). HBS-EP+ (10 mM HEPES [pH 7.4], 150 mM NaCl, 3 mM EDTA, and 0.05% [v/v] surfactant P20) containing 1.0% (v/v) DMSO was used as the running buffer for all experiments. Peptide binding was tested by injecting varying concentrations (0.3 nM to 1,000 nM) at a flow rate of 30 μl min^{-1} and measured by single cycle kinetics method. Raw data were analyzed by the BIACORE T100 evaluation software 2.01 and fitted to the standard 1:1 interaction model.

In Vitro Ubiquitin Transfer Assay by ^{35}S-Labeled E6AP HECT

E6AP HECT cDNA was subcloned into pTNT vector (Promega) at XhoI and SalI sites. ^{35}S-Methionine-labeled E6AP HECT was synthesized in vitro by TNT T7 coupled rabbit reticulocyte lysate system (Promega) at 30°C for 90 min, by following the standard procedure (Huibregtse et al., 1995). After translation, 0.5 μl of peptides in 10% (v/v) DMSO with 10× concentrations shown in Figure 4A were added to the translation reaction mixture (4.5 μL). The resulting mixture was incubated at room temperature at 30 min and

quenched with 2 × SDS-polyacrylamide gel laemli sample buffer (125 mM Tris-HCl [pH 6.8], SDS 4%, glycerol 20%, 0.002% bromophenol blue) in the absence of dithiothreitol. Samples were subjected to SDS-PAGE on a 10% polyacrylamide gel.

In Vitro Polyubiquitination Assay for Prx1 and p53

The plasmid pGEM p53 was used for in vitro translation (Werness et al., 1990). In vitro translation was performed using TNT T7 coupled rabbit reticulocyte lysate system. Recombinant baculovirus for HPV16 E6 was produced using the BaculoGold system (PharMingen) as described previously (Shirakura et al., 2007). Hi5 cells (Invitrogen) were infected with the recombinant baculovirus to produce HPV16 E6 protein. HPV16 E6 Protein was partially purified by anion-exchange chromatography as previously described (Huibregtse et al., 1993). In vitro polyubiquitination assays for Prx1 were performed essentially as described previously (Nasu et al., 2010). Hi5 cells were infected with recombinant baculoviruses AcMEF-E6AP and Ac MEF-E6AP^{C843A} to produce MEF-E6AP and MEF-E6AP^{C843A}, respectively (Shirakura et al., 2007). MEF-E6AP and MEF-E6AP^{C843A} were purified on anti-FLAG M2 agarose beads (Sigma) according to the manufacturer's instructions. Assays were done in 40 μl volumes containing 20 mM Tris (pH 7.6), 50 mM NaCl, 5 mM $MgCl_2$, 100 μM DTT, 5 mM ATP, 250 nM MEF-E6AP or inactive mutant MEF-E6AP^{C843A}, 62.5 nM $(His)_6$-E1, 1.1 μM $(His)_6$-UbcH7, 25 μM ubiquitin, 8 μM $(His)_6$-Prx1 and peptide, and incubation at 37°C for 30 min. Reactions were performed at 37°C for 30 min. The ubiquitination reaction was terminated by freezing the samples with liquid nitrogen. To dissociate proteins, 1% SDS was added to lysates, which were then heated at 90°C for 15 min. The samples were diluted 10-fold with a dissociation dilution buffer containing 1% NP-40, 0.5% deoxycholate, 120 mM NaCl, 50 mM HEPES, 1 mM EDTA, and complete protease inhibitor cocktail (Roche). Samples were immunoprecipitated with anti-Prx1 PAb and analysis by immunoblotting with antiubiquitin mouse monoclonal antibody (anti-Ubi-1, Millipore) to detect ubiquitinated Prx1. In vitro polyubiquitination assays for p53 were performed essentially as described previously (Nakagawa and Huibregtse, 2000). Assays were done in 75 μl volumes containing 25 mM Tris-HCl (pH 8.0), 125 mM NaCl, 2 mM $MgCl_2$, 50 μM DTT, 5 μM ubiquitin, 2 mM ATP, 170 nM MEF-E6AP, 33 nM $(His)_6$-E1, 0.6 μM $(His)_6$-UbcH7, 2 μl of partially purified HPV16 E6, and 5 μl of in vitro translated p53. Peptides inhibitors were added to the samples as indicated. The reaction mixtures were incubated at 37°C for 30 min. The ubiquitination reaction was terminated by freezing the samples with liquid nitrogen. To dissociate proteins, 1% SDS was added to lysates, which were then heated and diluted as described above. Samples were immunoprecipitated with anti-p53 rabbit polyclonal antibody (FL393, Santa Cruz), followed by immunoblotting with antiubiquitin mouse monoclonal antibody (anti-Ubi-1, Millipore) to detect ubiquitinated p53.

SUPPLEMENTAL INFORMATION

Supplemental Information includes four figures, one table, and supplemental Experimental Procedures and may be found with this article online at doi:10.1016/j.chembiol.2011.09.013.

ACKNOWLEDGMENTS

We thank Dr. Hiroshi Murakami for the discussion on conducting this work and Dr. Naoki Goshima for providing the cDNAs of E6AP and Smurf2. This work was supported by the Japan Society for the Promotion of Science (JSPS) Grants-in-Aid for the Specially Promoted Research (Grant 21000005), Research and Development Projects of the Industrial Science and Technology Program in the New Energy and Industrial Technology Development Organization (support to H.S.), Grants-in-Aid for JSPS Fellows (Grant 7734 to Y.Y.), JSPS Grants-in-Aid for Young Scientists (Grant B22710210 to T. Katoh and B22750145 to Y.G.), and Grants-in-Aid for Scientific Research from the Ministry of Health, Labour, and Welfare of Japan (to I.S. and H.S.).

Received: July 13, 2011
Revised: September 20, 2011
Accepted: September 20, 2011
Published: December 22, 2011

REFERENCES

Beaudenon, S., and Huibregtse, J.M. (2008). HPV E6, E6AP and cervical cancer. BMC Biochem. *9* (*Suppl 1*), S4.

Beaudenon, S., Dastur, A., and Huibregtse, J.M. (2005). Expression and assay of HECT domain ligases. Methods Enzymol. *398*, 112–125.

Biron, E., Chatterjee, J., Ovadia, O., Langenegger, D., Brueggen, J., Hoyer, D., Schmid, H.A., Jelinek, R., Gilon, C., Hoffman, A., and Kessler, H. (2008). Improving oral bioavailability of peptides by multiple N-methylation: somatostatin analogues. Angew. Chem. Int. Ed. Engl. *47*, 2595–2599.

Chatterjee, C., Paul, M., Xie, L., and van der Donk, W.A. (2005). Biosynthesis and mode of action of lantibiotics. Chem. Rev. *105*, 633–684.

Chatterjee, J., Gilon, C., Hoffman, A., and Kessler, H. (2008). N-methylation of peptides: a new perspective in medicinal chemistry. Acc. Chem. Res. *41*, 1331–1342.

Doedens, L., Opperer, F., Cai, M., Beck, J.G., Dedek, M., Palmer, E., Hruby, V.J., and Kessler, H. (2010). Multiple N-methylation of MT-II backbone amide bonds leads to melanocortin receptor subtype hMC1R selectivity: pharmacological and conformational studies. J. Am. Chem. Soc. *132*, 8115–8128.

Driggers, E.M., Hale, S.P., Lee, J., and Terrett, N.K. (2008). The exploration of macrocycles for drug discovery—an underexploited structural class. Nat. Rev. Drug Discov. *7*, 608–624.

Eldridge, A.G., and O'Brien, T. (2010). Therapeutic strategies within the ubiquitin proteasome system. Cell Death Differ. *17*, 4–13.

Eletr, Z.M., and Kuhlman, B. (2007). Sequence determinants of E2-E6AP binding affinity and specificity. J. Mol. Biol. *369*, 419–428.

Forster, A.C., Tan, Z., Nalam, M.N., Lin, H., Qu, H., Cornish, V.W., and Blacklow, S.C. (2003). Programming peptidomimetic syntheses by translating genetic codes designed *de novo*. Proc. Natl. Acad. Sci. USA *100*, 6353–6357.

Goto, Y., Ohta, A., Sako, Y., Yamagishi, Y., Murakami, H., and Suga, H. (2008). Reprogramming the translation initiation for the synthesis of physiologically stable cyclic peptides. ACS Chem. Biol. *3*, 120–129.

Goto, Y., Katoh, T., and Suga, H. (2011). Flexizymes for genetic code reprogramming. Nat. Protoc. *6*, 779–790.

Grünewald, J., and Marahiel, M.A. (2006). Chemoenzymatic and template-directed synthesis of bioactive macrocyclic peptides. Microbiol. Mol. Biol. Rev. *70*, 121–146.

Hershko, A., and Ciechanover, A. (1998). The ubiquitin system. Annu. Rev. Biochem. *67*, 425–479.

Hoeller, D., and Dikic, I. (2009). Targeting the ubiquitin system in cancer therapy. Nature *458*, 438–444.

Hoeller, D., Hecker, C.M., and Dikic, I. (2006). Ubiquitin and ubiquitin-like proteins in cancer pathogenesis. Nat. Rev. Cancer *6*, 776–788.

Huang, L., Kinnucan, E., Wang, G., Beaudenon, S., Howley, P.M., Huibregtse, J.M., and Pavletich, N.P. (1999). Structure of an E6AP-UbcH7 complex: insights into ubiquitination by the E2-E3 enzyme cascade. Science *286*, 1321–1326.

Huibregtse, J.M., Scheffner, M., and Howley, P.M. (1991). A cellular protein mediates association of p53 with the E6 oncoprotein of human papillomavirus types 16 or 18. EMBO J. *10*, 4129–4135.

Huibregtse, J.M., Scheffner, M., and Howley, P.M. (1993). Localization of the E6-AP regions that direct human papillomavirus E6 binding, association with p53, and ubiquitination of associated proteins. Mol. Cell. Biol. *13*, 4918–4927.

Huibregtse, J.M., Scheffner, M., Beaudenon, S., and Howley, P.M. (1995). A family of proteins structurally and functionally related to the E6-AP ubiquitin-protein ligase. Proc. Natl. Acad. Sci. USA *92*, 2563–2567.

Josephson, K., Hartman, M.C., and Szostak, J.W. (2005). Ribosomal synthesis of unnatural peptides. J. Am. Chem. Soc. *127*, 11727–11735.

Kawakami, T., Murakami, H., and Suga, H. (2008). Messenger RNA-programmed incorporation of multiple *N*-methyl-amino acids into linear and cyclic peptides. Chem. Biol. *15*, 32–42.

Kohli, R.M., Walsh, C.T., and Burkart, M.D. (2002). Biomimetic synthesis and optimization of cyclic peptide antibiotics. Nature *418*, 658–661.